Research Square

Preprints are preliminary reports that have not undergone peer review.
They should not be considered conclusive, used to inform clinical practice,
or referenced by the media as validated information.

Disulfiram Attenuates Paraquat-Induced Renal Injury and Fibrosis Associated with Modulation of Smad3/Smad7 Expression

Mahtab Esmaeili
Babol University of Medical Sciences
Abdolreza Daraei
Babol University of Medical Sciences
Hossein Najafzadehvarzi
Babol University of Medical Sciences
Soraya Khafri
Babol University of Medical Sciences
Zohre Esmaeili
Babol University of Medical Sciences
Yousef Beheshti
Babol University of Medical Sciences
Zahra Babazadeh
zbabazadeh1400@gmail.com

Babol University of Medical Sciences

Research Article

Keywords: Disulfiram, Paraquat, Renal Fibrosis, Oxidative Stress, Smad3, Smad7, Drug Repurposing

Posted Date: July 14th, 2026

DOI: https://doi.org/10.21203/rs.3.rs-10145851/v1

License: This work is licensed under a Creative Commons Attribution 4.0 International License.
Read Full License

Additional Declarations: No competing interests reported.

Version of Record: A version of this preprint was published at Molecular Biology Reports on October 25th, 2026. See the published version at https://doi.org/10.1007/s11033-026-13055-4.

Title: Disulfiram Attenuates Paraquat-Induced Renal Injury and Fibrosis Associated with Modulation of Smad3/Smad7 Expression

Running Title: Disulfiram Attenuates Paraquat-Induced Renal Fibrosis

Mahtab Esmaeili [1,2], Abdolreza Daraei [2,3], Hossein Najafzadehvarzi [2,4], Soraya Khafri [2,5] Zohre Esmaeili [2,6], Yousef Beheshti [1,3], Zahra Babazadeh [2,6*]

1-Student Research Committee, Babol University of Medical Sciences, Babol, Iran;

2-Cellular and Molecular Biology Research Center, Health Research Institute, Babol University of Medical Sciences, Babol, Iran

3-Department of Medical Genetics, School of Medicine, Babol University of Medical Sciences, Babol, Iran

4-Department of Pharmacology, Faculty of Medicine, Babol University of Medical Sciences, Babol, Iran.

5-Department of Epidemiology and Biostatistics, School of Public Health, Babol University of Medical Sciences, Babol, Iran

6-Department of Anatomical Sciences, School of Medicine, Babol University of Medical Sciences, Babol, Iran

Corresponding Author: Zahra Babazadeh

zbabazadeh1400@gmail.com

z.babazadeh@mubabol.ac.ir

Zahra Babazadeh ORCID: 0000-0002-0399-6937

Abdolreza Daraei ORCID: 0000-0002-2106-835X

Najafzadeh ORCID: 0000-0002-3686-7170

Soraya Khafri ORCID: 0000-0002-2398-7560

Zohre Esmaeili ORCID: 0009-0000-9919-4834

Abstract

Purpose: Paraquat (PQ) herbicide induces nephrotoxicity characterized by oxidative stress and fibrosis, contributing to chronic kidney disease. Drug repurposing offers a strategic approach for rapid therapeutic development. This study evaluated the nephroprotective potential of disulfiram (DSF), a clinically approved agent with emerging antioxidant and antifibrotic properties, against PQ-induced injury, focusing on the Smad3/Smad7 regulatory axis.

Methods: Thirty-five male Wistar rats were divided into seven groups: control, Vehicle, DSF20, PQ (1.5 mg/kg), and PQ co-treated with DSF (5, 10, or 20 mg/kg). Renal injury was assessed via histopathology (H&E, PAS, Masson's trichrome), serum biomarkers (BUN, creatinine, uric acid), oxidative stress markers (MDA levels, CAT and GPx activities), and gene expression of Smad3 and Smad7 (qRT-PCR).

Results: PQ administration caused significant histopathological damage, elevated oxidative stress (increased MDA, altered CAT/GPx), upregulated profibrotic Smad3, and impaired renal function. DSF co-treatment, particularly at 10 mg/kg, markedly attenuated these effects. It reduced tissue fibrosis and inflammation, restored antioxidant enzyme activity, decreased lipid peroxidation, and rebalanced Smad signaling by downregulating Smad3 while upregulating Smad7. Normalized BUN and uric acid levels evidenced functional improvement.

Conclusion: Disulfiram at an optimal dose of 10 mg/kg confers significant renoprotection against paraquat nephrotoxicity by mitigating oxidative stress and is associated with modulation of Smad3/Smad7 expression. These findings identify DSF as a promising repurposed drug candidate for preventing pesticide-induced renal fibrosis.

Keywords: Disulfiram; Paraquat; Renal Fibrosis; Oxidative Stress; Smad3; Smad7; Drug Repurposing

Introduction

Fibrosis represents a maladaptive response to repetitive tissue injury and incomplete repair, particularly under chronic inflammatory conditions, and accounts for nearly 45% of deaths in industrialized nations (Chung et al., 2013). Once considered irreversible, fibrosis is now recognized as a dynamic and progressive process. Within the kidneys, fibrosis is the defining feature of chronic kidney disease (CKD), which affects 10–13% of the global population and significantly increases cardiovascular risk (Kalantar-Zadeh, Jafar, Nitsch, Neuen, & Perkovic, 2021). Regardless of etiology, CKD progression ultimately converges on fibrosis, characterized by extracellular matrix (ECM) remodeling, parenchymal scarring, and functional decline (Rieder et al., 2025).

Among environmental toxins, paraquat—a widely used herbicide despite global restrictions (Tayeb, Felemban, Adnan Ashour, & Shafie, 2024)—represents a major nephrotoxic threat (Isha et al., 2018; Zhang et al., 2024). Human exposure can occur accidentally through contaminated food or intentionally via self-poisoning (Shadnia et al., 2018; Zou, He, Cao, & Li, 2015). Paraquat induces the generation of reactive oxygen species (ROS), mitochondrial dysfunction, and apoptosis, with the kidneys serving as a major site of accumulation and injury. This tubular damage results in oliguria and elevated serum creatinine levels (McGwin Jr & Griffin, 2022; Nouri, Ghorbani, & Shahriary, 2025). Critically, no effective antidote exists, and even chronic low-level exposure can sustain toxic blood concentrations (Sittipunt, 2005; Wang et al., 2020). These features establish paraquat as both a significant human nephrotoxin and a widely used experimental tool for inducing renal fibrosis in animal models (Nouri et al., 2025; Z. Wang et al., 2024; Zhang et al., 2024)

The pathogenesis of renal fibrosis is orchestrated by a constellation of dysregulated signaling pathways, with the TGF-β/Smad axis occupying a central and well-established role (Huang, Fu, & Ma, 2023; Yu, Sun, Zhang, Zou, & Zhao, 2022). As a master regulator, TGF-β1 drives the core pathological features of fibrosis, including renal cell apoptosis, excessive ECM deposition, and myofibroblast trans-differentiation (Juan et al., 2023; Y. Wang et al., 2024). However, the pleiotropic nature of TGF-β signaling presents a significant therapeutic challenge; its systemic inhibition, while antifibrotic, concurrently disrupts vital homeostatic functions, thereby constraining direct clinical targeting (Hong et al., 2025; Jing, Gao, Jing, Yang, & Liu, 2025; Wal et al., 2025). This conundrum has pivoted therapeutic focus toward downstream, more disease-specific effectors.

Among these, **Smad3** serves as the principal transcriptional engine of TGF-β-driven fibrogenesis. Its profibrotic activity is potentiated by intracellular ROS (Dituri, Cossu, Mancarella, & Giannelli, 2019). An opposing protective role is fulfilled by **Smad7**, an endogenous inhibitor that attenuates signaling by targeting the TGF-β receptor complex for degradation, thus forming a critical self-regulatory circuit (Jiao, Zhang, Chen, & Zhang, 2025; Zhanga & Wub, 2025). The fibrogenic output is further governed by a higher-order balance between the TGF-β/Smad and bone morphogenetic protein (BMP) pathways. Specifically, BMP7 antagonizes TGF-β/Smad3-driven fibrosis via Smad1/5/8 activation and Smad7, which restores expression of antifibrotic microRNAs (e.g., miR-29, miR-200) and impedes Smad3 nuclear translocation (Dituri et al., 2019; Meng, Chung, & Lan, 2013). Consequently, the pathologically imbalanced Smad3/Smad7 ratio—marked by Smad3 hyperactivation and Smad7 suppression—has

emerged as a hallmark of progressive fibrosis (Gu, Liu, & Lan, 2024; Zhanga & Wub, 2025). Consequently, the pathologically imbalanced **Smad3/Smad7 ratio**—marked by Smad3 hyperactivation and Smad7 suppression—has emerged as a hallmark of progressive fibrosis. This insight rationalizes a refined therapeutic paradigm: interventions designed to selectively inhibit Smad3 activity or restore Smad7 function present a more precise and potentially safer strategy to mitigate fibrosis while preserving the beneficial pleiotropy of TGF-β.

In this context, disulfiram (DSF), an FDA-approved drug for alcohol addiction, has emerged as a candidate for drug repurposing due to its pleiotropic anti-fibrotic effects (Okabe et al., 2024; Yang et al., 2022). Beyond its classical use, DSF and its metabolite demonstrate multi-targeted actions, including potent antioxidant activity, inhibition of lysyl oxidase (LOX)–mediated collagen crosslinking (Saifi & Godugu, 2022; Saifi, Shaikh, Kaki, & Godugu, 2022), and upregulation of matrix metalloproteinases (MMPs) that promote collagen degradation (Hassan et al., 2019; Hassan, Ebaid, Alhazza, Al-Tamimi, & Rady, 2023). Importantly, these mechanisms may directly converge upon the TGF-β/Smad axis. Given that oxidative stress is a known activator of Smad3 (Zhanga & Wub, 2025). DSF's antioxidant properties could indirectly suppress Smad3 phosphorylation and activity. Furthermore, by modulating the cellular redox state, DSF might create a milieu favorable for Smad7 expression and stability, thereby rebalancing the Smad3/Smad7 ratio. Preclinical studies provide strong evidence for its efficacy in models of lung, liver, and kidney fibrosis at doses ranging from 1 to 100 mg/kg (Hamidi et al., 2023; Saifi et al., 2022; Yang et al., 2022), Yet its specific impact on the Smad3/Smad7 regulatory balance in the context of nephrotoxicity remains unexplored.

Given that fibrosis is the final common pathway in CKD progression and that paraquat is a potent inducer of renal fibrosis, the present study was designed to investigate the nephroprotective potential of disulfiram against paraquat-induced injury. We specifically hypothesized that DSF attenuates paraquat-induced renal fibrosis by reducing oxidative stress and, more critically, by downregulating the pro-fibrotic Smad3 while upregulating the inhibitory Smad7, thereby restoring the homeostatic Smad3/Smad7 balance. By targeting downstream TGF-β/Smad signaling while leveraging an FDA-approved drug, this study positions disulfiram as a promising repurposed candidate for mitigating pesticide-induced renal fibrosis.

2. **Materials and Methods**

2.1. Animal Care and Experimental Design

2.1.1. Animal Care and Housing

All animal procedures were approved by the Institutional Animal Care and Use Committee (Approval code: IR.MUBABOL.AEC.1402.028). and were conducted in accordance with institutional guidelines for the care and use of laboratory animals (Clinical trial number: Not applicable). A total of 35 healthy male Wistar rats (8 ± 1 weeks old, 200 ± 20 g) were obtained from the Laboratory Animal Center. Animals were housed under controlled environmental conditions (22 ± 3 °C; 55 ± 10% humidity; 12 h light/dark cycle), with free access to standard rodent chow (Pars Animal Feed Co., Tehran, Iran) and tap water. All efforts were made to minimize animal suffering and reduce the number of animals used.

2.1.2. Paraquat-Induced Renal Fibrosis Model and Experimental Design

Thirty-five rats were randomly divided into seven groups (n = 5 each):

Group	Treatment	Dose	Route
I (Control)	No Treatment	-	-
II (Vehicle)	Olive oil	200µl/day	i.p.
III (DSF20)	Disulfiram alone	20mg/kg/day	i.p.
IV (PQ)	Paraquat	1.5 mg/kg/day	p.o
V (PQ+DSF5)	Paraquat + Disulfiram	1.5 + 5 mg/kg/day	p.o + ip
VI (PQ+DSF10)	Paraquat + Disulfiram	1.5 + 10 mg/kg/day	p.o + ip
V (PQ+DSF20)	Paraquat + Disulfiram	1.5 + 20 mg/kg/day	p.o + ip

The paraquat dose was selected based on Awadalla (2012) (Awadalla, 2012), who demonstrated that this regimen induces marked renal fibrosis within 4 weeks, characterized by increased collagen deposition and upregulation of profibrotic markers. The DSF medium dose (10 mg/kg/day, i.p.) was selected based on previous studies demonstrating anti-fibrotic efficacy in rodent models of lung (Hamidi et al., 2023; Karimzadeh et al., 2025); Low (5 mg/kg) and high (20 mg/kg) doses were included to evaluate dose-dependent effects. All treatments were administered once daily, 5 consecutive days per week, with 2-day intervals, for a total of 4 weeks.

2.1.3. Euthanasia and Tissue Collection

At the end of the experimental period, rats were anesthetized via intraperitoneal injection of ketamine (80 mg/kg) and xylazine (10 mg/kg). Following confirmation of deep anesthesia (lack of response to toe pinch), euthanasia was ensured via exsanguination during cardiac puncture and confirmed by bilateral thoracotomy.

Blood was collected via cardiac puncture at a 20–30° angle toward the point of maximal heartbeat. Samples were allowed to clot at room temperature for 30 min and centrifuged at 3000 rpm for 15 min to obtain serum, which was stored at −80 °C until analysis. Both kidneys were immediately excised: the right kidney was fixed in 10% neutral-buffered formalin for 72 h for histological assessment, and the left kidney was snap-frozen in liquid nitrogen and stored at −80 °C for molecular and biochemical analyses.

2.2. Histopathological Assessments

2.2.1 Tissue Processing and Staining

Fixed kidney tissues were processed through graded ethanol solutions (70%, 80%, 90%, 96%, and 100%), cleared in xylene, and embedded in paraffin wax. Serial sections (3 μm) were cut using a rotary microtome (Leica RM2245, Germany) and mounted on glass slides.

For histopathological assessment, sections were stained with:

Hematoxylin and Eosin (H&E): Following deparaffinization and rehydration, sections were stained with Mayer's hematoxylin and eosin Y (Asiapajouhesh, Iran) according to standard protocols (Hasan, Das, & Chowdhury, 2021).

Masson's Trichrome: Collagen deposition was assessed using a commercial kit (Asiapajouhesh, Iran; Cat. No. 140011) as per the manufacturer's instructions (Sridharan et al., 2022).

Periodic Acid-Schiff (PAS): Staining was performed using 0.5% periodic acid and Schiff's reagent to visualize basement membranes (Zakout, Abdellah, Abdallah, & Batran, 2024).

Detailed staining protocols are provided in Supplementary Method S1.

2.2.2. Semi-Quantitative Histopathological Analysis:

Kidney weight and volume (by water displacement) were recorded (Saleh, Mahmoud, Al-Salahy, & Mohamed Moustafa, 2023).Histopathological evaluation was performed in a blinded manner using an Olympus BX53 microscope. Digital images were captured with an AmScope camera and analyzed using Zistrad software.

A semi-quantitative scoring system (0: absent, 1: mild, 2: moderate, 3: severe) was applied to assess key lesions in H&E-stained sections, including: Tubular necrosis, Intratubular casts, Glomerular hyper-segmentation, Bowman's space dilation, Inflammatory infiltrates, and Congestion. The scoring criteria for each lesion followed previously published standards (Agrawal & Gowrishankar, 2024; Prayaga et al., 2011). Glomerular integrity was quantified by counting intact, hyper-segmented, and necrotic renal corpuscles in 25 non-overlapping, randomly selected cortical fields per animal at 18× magnification.

PAS-stained sections were evaluated for basement membrane thickening, and Masson’s trichrome-stained sections were used to quantify interstitial fibrosis (Chen, Li, & Ni, 2019; Hoshino et al., 2015).

2.2.3 Fibrosis Quantification (Histomorphometry)

Renal interstitial fibrosis was quantified histomorphometrically on Masson's trichrome-stained tissue sections. Using Fiji (ImageJ) software (National Institutes of Health, USA), collagen was specifically isolated by color deconvolution using the "Masson's Trichrome" vector. The collagen-positive area (stained blue) was measured in five randomly selected, non-overlapping fields per animal at 18× magnification. Fields were selected using the systematic random sampling method described above. The collagen-positive area was expressed as a percentage of the total field area. Representative images are shown in Figure S1.

2.3. Molecular Analyses

2.3.1. Gene Expression Analysis (Smad3 and Smad7)

Total RNA was isolated from frozen kidney tissues (~30 mg) using lysis buffer (Parstous, Mashhad, Iran). RNA concentration and purity were determined spectrophotometrically (NanoDrop, Thermo Fisher Scientific, USA), and integrity was verified by agarose gel electrophoresis.

First-strand cDNA was synthesized from 1 µg of total RNA using a commercial reverse transcription kit (YTA, Iran) in a 20 µL reaction volume. qRT-PCR was performed in triplicate with SYBR Green Master Mix (Ampliqon, Denmark) in a final volume of 20 µL containing 2 µL of cDNA template and 0.5 µM of each primer on a Mic qPCR Cycler (Bio Molecular Systems, Australia). The cycling protocol included: initial denaturation (95 °C, 15 min), followed by 40 cycles of denaturation (95 °C, 30 s), annealing (Smad3: 64 °C; Smad7: 61 °C; GAPDH: 58 °C; 30 s), and extension (72 °C, 30 s).

Melting curve analysis confirmed the specificity of amplification. Expression levels were normalized to GAPDH and quantified by the 2^(-ΔΔCT) method. Primer sequences are shown in Table 1.

Table 1. Primer sequences used in qRT-PCR

Gene	Forward (5′–3′)	Reverse (5′–3′)
Smad3	TTTCGTCCAGTCTCCCAACT	GTAGACAGCCTCAAAGCCCT
Smad7	TGAAACCGGGGGAACGAAT	AGGGCTCTTGGACACAGTAGA
GAPDH	GACAGCCGCATCTTCTTGTG	GGTAACCAGGCGTCCGATAC

2.4. Biochemical Analyses

2.4.1. Serum Kidney Function Markers

Serum levels of blood urea nitrogen (BUN), creatinine (Cr), and uric acid (UA) were measured using colorimetric assay kits (Pars Azmoon, Tehran, Iran) according to the manufacturer's protocols. All measurements were performed in duplicate.

2.4.2. Oxidative Stress Markers

Kidney tissues were homogenized (10% w/v) in ice-cold phosphate-buffered saline (PBS, pH 7.4) using a glass-Teflon homogenizer. The homogenate was centrifuged at 12,000 rpm for 15 min at 4 °C, and the supernatant was used for oxidative stress assays.

Catalase (CAT) activity was measured using a commercial kit (Kiazist, Hamedan, Iran) based on the decomposition of hydrogen peroxide (H_2O_2), measured at 240 nm.

Malondialdehyde (MDA) levels (a marker of lipid peroxidation) were determined using the thiobarbituric acid reactive substances (TBARS) method with a commercial kit (Kiazist, Hamedan, Iran).

Glutathione peroxidase (GPx) activity was measured using a kit from Navand Salamat (Urmia, Iran), which quantifies the reduction of cumene hydroperoxide coupled with NADPH oxidation

2.5. Statistical Analysis

All experimental data, including histopathological assessments, enzymatic activity measurements, and Smad3/Smad7 gene expression levels, were statistically analyzed using GraphPad Prism software (version 10.4.1).

Histopathological scoring of renal tissue lesions (semi-quantitative grades 0–3) was analysed using the nonparametric Kruskal–Wallis test. followed by Dunn's post-hoc test for pairwise comparisons..

Quantitative data from gene expression analyses and enzymatic assays were evaluated by one-way analysis of variance (ANOVA). Following a significant ANOVA result, multiple comparisons among group means were performed using Tukey’s honest significant difference (HSD) post-hoc test.

Statistical significance was defined as a two-tailed p-value < 0.05 for all analyses.

3. Results

3.1. Kidney Weight and Volume

Paraquat (PQ) intoxication significantly reduced kidney weight compared to the control group (0.94 ± 0.05 g vs. 1.38 ± 0.12 g, $P = 0.010$). Coadministration of DSF at a dose of 10 mg/kg (PQ+DSF10) significantly attenuated this reduction (1.34 ± 0.09 g, $P = 0.037$ vs. PQ group). In contrast, kidney volume did not show any statistically significant alterations among the experimental groups (Figure 1a, b).

3.2. Renal Corpuscle Counts

3.2.1. Intact Renal Corpuscles Count

Intact renal corpuscles were significantly reduced in the PQ group relative to controls (3.4 ± 0.3 vs. 6.10 ± 0.29, P < 0.0001). Coadministration of DSF at 10 mg/kg and 20 mg/kg significantly restored their numbers (6.02 ± 0.24, P < 0.0001 and 5.62 ± 0.31, P = 0.0003, respectively, vs. PQ group). The count in the PQ+DSF5 group (3.29 ± 0.34) remained comparable to the PQ group but was significantly lower than in both higher-dose DSF groups (P < 0.0001 and P = 0.0005, respectively).

3.2.2. Necrotic Renal Corpuscles Count

Necrotic renal corpuscles were significantly increased by PQ exposure (1.96 ± 0.2 vs. 0.5 ± 0.14 in controls, P < 0.0001). This increase was attenuated by DSF at 10 mg/kg (0.6 ± 0.12, P < 0.0001 vs. PQ) and 20 mg/kg (1.18 ± 0.16, P = 0.046 vs. PQ).

3.2.3. Hyper-segmented Renal Corpuscles Count

Hyper-segmented renal corpuscles were also markedly elevated in the PQ group (3.07 ± 0.17 vs. 0.83 ± 0.19 in controls, P < 0.0001). All DSF co-treatment groups (PQ+DSF5: 1.2 ± 0.2; PQ+DSF10: 0.91 ± 0.12; PQ+DSF20: 1.1 ± 0.17) significantly reduced this pathology compared to the PQ group (P < 0.0001 for all) (Figure 2a,b,c).

3.3. Semi-Quantitative Histopathological Scoring

3.3.1. Cortical Structural Damage

Cortical structural damage was significantly elevated in the PQ group compared to controls (2.84 ± 0.05 vs. 0.20± 0.09, P < 0.0001). DSF co-treatment dose-dependently reduced this damage, with significant improvements in the PQ+DSF5 (1.76 ± 0.15, P = 0.009), PQ+DSF10 (0.66 ± 0.1, P < 0.0001), and PQ+DSF20 (1.14 ± 0.1, P < 0.0001) groups relative to the PQ group. The PQ+DSF10 group also showed significantly less damage than the PQ+DSF5 group (P = 0.009). (Figure 3a and Figure 4, Supplementary Table 1).

3.3.2. Medullary Structural Injury

Medullary structural injury followed a similar pattern, with PQ inducing a significant increase in damage score (2.7 ± 0.09 vs. 0.14 ± 0.06, P < 0.0001). This injury was significantly attenuated by DSF at doses of 10 mg/kg (1.40± 0.12, P = 0.002) and 20 mg/kg (1.52± 0.15, P = 0.006). (Figure 3b and Figure 5, Supplementary Table 1).

3.3.3. Cellular Morphological Alterations in Tubular Epithelium

Cellular morphological alterations in tubular epithelium were markedly increased by PQ (2.24 ± 0.09 vs 0.26 ± 0.06, $P < 0.0001$). All DSF co-treatment groups significantly mitigated these alterations (PQ+DSF5: 1.28 ± 0.12, $P = 0.0007$; PQ+DSF10: 0.46 ± 0.08, $P < 0.0001$; PQ+DSF20: 0.95 ± 0.16, $P < 0.0001$; all vs. PQ group). The protective effect was strongest in the PQ+DSF10 group, which outperformed the PQ+DSF5 group ($P = 0.0003$). (Figure 3c and Figure 4, Supplementary Table 1).

3.3.4. Vascular Congestion

Vascular congestion was significantly exacerbated by PQ (2.47 ± 0.11 vs. 0.43± 0.15, $P < 0.0001$). DSF at 10 mg/kg and 20 mg/kg effectively reduced congestion scores (0.21 ± 0.07, $P < 0.0001$ and 1.57 ± 0.09, $P = 0.006$, respectively, vs. the PQ group). The PQ+DSF10 group demonstrated a superior effect compared to both the PQ+DSF5 and PQ+DSF20 groups ($P < 0.0001$). (Figure 3d and Figure 4, Supplementary Table 1).

3.3.5. Interstitial Inflammatory Infiltration

Interstitial inflammatory infiltration was elevated in the PQ group (1.02 ± 0.13 vs. 0.3043 ± 0.09, $P = 0.004$). Among the treatment groups, only DSF at 10 mg/kg significantly reduced the infiltration (0.39 ± 0.07, $P = 0.004$ vs. PQ group), showing greater efficacy than the PQ+DSF5 group ($P = 0.0003$). (Figure 3e, Supplementary Table 1).

3.3.6. Urinary Space Expansion

Urinary space expansion was significantly increased by PQ administration (2.89 ± 0.05 vs. 0.2813 ± 0.08, $P < 0.0001$). Co-treatment with DSF at 10 mg/kg and 20 mg/kg substantially reduced this expansion (1.11 ± 0.12, $P < 0.0001$, and 1.68 ± 0.09, $P < 0.0001$, respectively, vs. the PQ group). The PQ+DSF10 group showed a lower score than the PQ+DSF5 group ($P = 0.002$). Notably, DSF administered alone also induced a mild but significant expansion compared to control ($P = 0.005$), though to a far lesser extent than PQ ($P < 0.0001$). (Figure 3f and Figure 4, Supplementary Table 1).

3.3.7. Glomerular Basement Membrane (GBM) Thickening

Glomerular basement membrane (GBM) thickening was markedly induced by PQ (2.46 ± 0.09 vs. 0.08 ± 0.05, P < 0.0001). This thickening was significantly attenuated only by co-treatment with DSF at 10 mg/kg (0.84 ± 0.11, P < 0.0001 vs. PQ group). (Figure 6 and Figure 7, Supplementary Table 1).

3.4. Renal Fibrosis Analysis

3.4.1. Fibrosis Across Compartments (Glomerular, Interstitial, Perivascular, Medullary)

Renal fibrosis was significantly increased by PQ administration across all assessed compartments. **Glomerular fibrosis** was markedly elevated in the PQ group (2.21 ± 0.06, 0.46 ± 0.09, P < 0.0001) and significantly reduced by co-treatment with DSF at 10 mg/kg (1.19 ± 0.10, P < 0.0001 vs. PQ), but not at 5 and 20 mg/kg (P=>0.9999, P = 0.094, respectively).

Interstitial fibrosis was also profoundly increased by PQ. While co-treatment with DSF at both 10 mg/kg and 20 mg/kg significantly attenuated PQ-induced interstitial fibrosis (0.30 ± 0.07, P < 0.0001 and 0.76 ± 0.16, P = 0.002, respectively, vs. PQ group).

Perivascular fibrosis was exacerbated by PQ (1.9 ± 0.18 vs. 0.23 ± 0.10, P < 0.0001), and only DSF at 10 mg/kg significantly mitigated this effect (0.43 ± 0.12, P = 0.0001 vs. PQ group).

Medullary fibrosis followed a similar pattern, with PQ causing significant damage (2.93 ± 0.06 vs. 0.12 ± 0.08, P < 0.0001), P < 0.0001). Co-treatment with DSF at 10 mg/kg significantly reduced fibrosis compared to the PQ group (1.11 ± 0.16, P = 0.0001). (data in Table 1 and illustrated in Figures 8 & 9). (Figure 8a-d and Figure 10, Supplementary Table 1).

3.4.2. Digital Morphometric Analysis for Renal Fibrosis Percentage

The percentage of renal fibrosis was significantly increased by PQ administration compared to the control group (29.38 ± 1.345% vs. 5.164 ± 0.3894%; P < 0.0001). Co-treatment with DSF at all tested doses (5, 10, and 20 mg/kg) significantly attenuated this fibrotic response compared to the PQ group (P < 0.0001). Comparative analysis among the DSF-treated groups revealed that the intermediate dose of 10 mg/kg (PQ+D10: 7.833 ± 0.5609%) produced the most significant anti-fibrotic effect. This was evidenced by its superior efficacy relative to both the lower dose of 5

mg/kg (PQ+D5: 17.61 ± 1.030%; P < 0.0001) and the higher dose of 20 mg/kg (PQ+D20: 13.17 ± 0.6781%; P < 0.0001). The difference between the PQ+D5 and PQ+D20 groups was also statistically significant (P = 0.0018) (Figures 9 and 10).

3.5. Expression of Profibrotic and Antifibrotic Mediators (Smad3 and Smad7)

Smad3 mRNA expression was significantly upregulated in the PQ group compared to the control group (1.51 ± 0.15; P = 0.029 vs. 1.00 ± 0.05; P = 0.028). Co-treatment with DSF at all tested doses significantly downregulated this expression relative to the PQ group: PQ+DSF5 (0.86 ± 0.11, P = 0.003), PQ+DSF10 (0.70 ± 0.08, P = 0.0002), and PQ+DSF20 (0.55 ± 0.10, P < 0.0001). DSF administered alone at 20 mg/kg also significantly reduced Smad3 expression compared to the control (0.24 ± 0.06; P = 0.0003).

Smad7 mRNA expression was not significantly altered in the PQ group compared to controls (0.64 ± 0.10 vs. 1.10 ± 0.26; P = 0.8715). However, co-treatment with DSF at 10 mg/kg (PQ+DSF10) significantly increased Smad7 expression relative to the PQ group (2.45 ± 0.39, P = 0.0006). Furthermore, Smad7 expression in the PQ+DSF10 group was significantly higher than in the PQ+DSF5 group (0.79 ± 0.08, P = 0.002). (Figure 11a,b, Supplementary Table 2 and 3

3.6. Oxidative Stress Markers

3.6.1. Glutathione peroxidase (GPx):

GPx activity was significantly elevated in the PQ group compared to the control (P = 0.0003). This elevation was markedly reduced by co-administration of DSF at 5 mg/kg (P < 0.0001 vs. PQ group). In contrast, DSF at 20 mg/kg in combination with PQ further increased GPx activity, resulting in levels significantly higher than both the control and DSF-alone groups (P < 0.0001 and P = 0.009, respectively).

3.6.2. Catalase (CAT):

CAT activity was significantly increased in both the DSF20-alone group (P < 0.0001 vs. control) and the PQ group (P = 0.0002 vs. control). Among the co-treatment groups, DSF at 20 mg/kg exerted the most pronounced effect,

elevating CAT activity significantly above that of the PQ group, as well as the PQ+DSF5 and PQ+DSF10 groups (all $P < 0.0001$).

3.6.3. Malondialdehyde (MDA) levels:

MDA levels, a marker of lipid peroxidation, were significantly increased by PQ administration ($P = 0.003$ vs. control). Co-treatment with DSF at 5 mg/kg and 10 mg/kg significantly reduced MDA levels compared to the PQ group ($P = 0.028$ and $P = 0.002$, respectively). Furthermore, MDA levels in the PQ+DSF10 group were significantly lower than in the PQ+DSF20 group ($P = 0.034$). (Table 1)

3.7. Renal Function Biomarkers

3.7.1. Blood Urea Nitrogen (BUN):

BUN levels were significantly elevated in the PQ group compared to the control group ($P < 0.0001$). Co-treatment with disulfiram significantly reduced BUN levels at all doses relative to the PQ group ($P < 0.0001$ for PQ+DSF5 and PQ+DSF10; $P = 0.006$ for PQ+DSF20).

3.7.2. Creatinine:

No statistically significant differences in serum creatinine levels were observed among any of the experimental groups ($P = 0.500$).

3.7.3. Uric Acid (UA):

UA concentrations were significantly increased in the PQ group relative to controls ($P = 0.012$). Co-administration of disulfiram at 5 mg/kg and 10 mg/kg significantly reduced UA levels compared to the PQ group (both $P < 0.0001$). Furthermore, UA levels in the PQ+DSF5 and PQ+DSF10 groups were significantly lower than in the PQ+DSF20 group ($P < 0.0001$). (Table 2)

4. Discussion

Despite its well-documented high toxicity and associated bans or restrictions, paraquat remains a widely used herbicide. Its nephrotoxicity primarily stems from the induction of severe oxidative stress, leading to cellular and tissue damage, a process centrally mediated by ROS, cytokine-driven inflammation, and signaling pathways such as

TGF-β/BMP/Smad (Dituri et al., 2019; Gu, Liu, Huang, Yu, & Lan, 2020; Meng et al., 2013; Subbiah & Tiwari, 2021; Zhang et al., 2024). This study investigated the renoprotective potential of disulfiram—a drug with a clinical history in alcoholism treatment and emerging anti-inflammatory and antifibrotic properties—in an experimental model of PQ-induced renal injury. We employed a multi-faceted approach, integrating histopathological analysis, gene expression profiling of key Smad regulators, assessment of antioxidant enzyme activities, and evaluation of renal function markers. Our primary objectives were to elucidate DSF's capacity to mitigate fibrosis, oxidative stress, and structural kidney damage, and to identify its optimal therapeutic dose.

4.1. Histopathological Evidence of Paraquat-Induced Injury and Disulfiram's Protective Effects

Our histopathological findings align with established literature, demonstrating that PQ administration induces extensive architectural disruption in the kidney, prominently affecting glomeruli, Bowman's capsule, and interstitial regions (Agrawal & Gowrishankar, 2024; Prayaga et al., 2011). Similar to previous studies, our observations included significant glomerular necrosis and hyper-segmentation, tubular damage, interstitial inflammatory infiltration, vascular congestion, and capsular space expansion. These alterations signify severe vascular compromise and tissue disorganization. The central mechanism driving this damage is PQ-induced oxidative stress. Paraquat undergoes redox cycling, primarily via mitochondrial complexes I and III and interactions with enzymes like NADPH oxidase (NOX), leading to massive ROS generation and peroxynitrite ($ONOO^-$) formation (Sittipunt, 2005; Sule, Condon, & Gomes, 2022). This oxidative assault results in lipid peroxidation, protein/DNA damage, and ultimately, necrosis and fibrosis.

Disulfiram co-treatment, particularly at the 10 mg/kg dose (PQ+DSF10), significantly attenuated these histopathological injuries, suggesting a potent tissue-reparative effect. The lower dose (5 mg/kg) showed a heterogeneous response, improving some parameters (e.g., cortical disarray, glomerular necrosis) but not others (e.g., capsular space expansion, medullary disorganization). The higher dose (20 mg/kg) provided significant protection in several histopathological parameters compared to the PQ group, though its efficacy in mitigating inflammation and basement membrane thickening was less pronounced than the 10 mg/kg dose. Importantly, DSF administered alone did not induce histopathological changes, indicating its safety at the tested dose. These findings are supported by studies in other renal injury models, where DSF reduced tubular degeneration, inflammatory infiltration, and glomerular necrosis (Cai et al., 2022; Toda et al., 2022). The structural improvements were

paralleled by significant reductions in serum BUN and uric acid levels, indicating a concordant restoration of renal function.

4.2. Modulation of Oxidative Stress and Antioxidant Defense

The oxidative burden was confirmed by a significant increase in lipid peroxidation (MDA levels) in the PQ group. DSF co-treatment, especially at 10 mg/kg, effectively reduced MDA, aligning with its proposed antioxidant role (Bahramibanan, Rad, Ranjbar, Karbasi, & Abbasifard, 2025).

Analysis of antioxidant enzymes revealed a complex, dose-dependent response. Activities of glutathione peroxidase (GPx) and catalase (CAT) were significantly elevated in the PQ group compared to the control. This upregulation likely represents a compensatory cellular attempt to neutralize excess ROS (de Haan et al., 1998; Pei, Pan, Wei, & Hua, 2023). The response to DSF co-treatment varied by dose. The 5 mg/kg dose (PQ+DSF5) significantly lowered GPx activity compared to PQ, possibly indicating a reduced need for compensatory upregulation as DSF mitigates the primary oxidative insult. The 10 mg/kg dose (PQ+DSF10) restored both GPx and CAT activities close to the control range, suggesting an optimal rebalancing of the redox state. In contrast, the 20 mg/kg dose (PQ+DSF20) provoked the highest GPx and CAT activities, potentially indicating a pro-oxidant shift or metabolic disturbance at this higher dose, which then triggered a renewed compensatory antioxidant response (Guo, Chen, Li, Xu, & Wang, 2022). This dose-dependent effect on antioxidant enzymes underscores the importance of dose optimization for DSF's therapeutic window and highlights its primary action in reducing oxidative burden.

4.3. Smad3/Smad7 Modulation as a Putative Antifibrotic Mechanism

A pivotal finding of this study is the modulation of the Smad3/Smad7 axis by DSF. PQ intoxication led to a significant upregulation of the profibrotic gene *Smad3*. Co-treatment with DSF at all doses (5, 10, and 20 mg/kg) significantly suppressed this PQ-induced *Smad3* overexpression. Concurrently, the 10 mg/kg dose uniquely and significantly upregulated the expression of the inhibitory *Smad7* gene compared to both the PQ and PQ+DSF5 groups. This dual action—suppressing the effector (*Smad3*) and enhancing the inhibitor (*Smad7*)—suggests a role in rebalancing this regulatory axis, crucial for controlling fibrogenesis (Jiang et al., 2021; Wu, Wang, Yu, & Lan, 2022).

This molecular evidence directly correlates with the observed histopathological outcomes. The significant reduction in glomerular, interstitial, perivascular, and medullary fibrosis and the percentage of interstitial fibrosis across all

DSF-treated groups is consistent with the observed downregulation of Smad3. The superior histological protection and specific upregulation of *Smad7* at the 10 mg/kg dose highlight its optimal efficacy. Our results are consistent with other models where antifibrotic agents, including DSF, exerted protection by rebalancing Smad3/Smad7 signaling (Mallone et al., 2021; Saifi & Godugu, 2022). The observed effects may be mediated through modulation of TGF-β/Smad signaling and reduction of oxidative stress, both of which are implicated in renal fibrogenesis (Du et al., 2023; Li et al., 2018; Xiong et al., 2025). Consequently, the amelioration of functional markers (BUN, UA) is likely secondary to this combined structural and molecular protection.

Based on the present findings, a putative mechanism underlying the renoprotective effects of disulfiram can be proposed. Paraquat exposure is known to induce excessive oxidative stress, leading to lipid peroxidation and activation of inflammatory and profibrotic signaling pathways. Increased Smad3 expression together with reduced Smad7 expression may contribute to extracellular matrix accumulation and renal fibrosis. In the present study, disulfiram treatment was associated with reduced oxidative stress, restoration of antioxidant defense, and modulation of Smad3 and Smad7 expression, which may collectively contribute to attenuation of renal fibrosis and preservation of renal structure and function. A schematic representation of this proposed mechanism is presented in Figure 12.

5. Conclusion

In conclusion, our integrative analysis demonstrates that disulfiram, particularly at a dose of 10 mg/kg, provides significant protection against paraquat-induced nephrotoxicity. Its beneficial effects were associated with attenuation of histopathological injury, reduction of oxidative stress and lipid peroxidation, normalization of antioxidant responses, and modulation of Smad3 and Smad7 expression. These coordinated effects were accompanied by reduced renal fibrosis and improvement of functional markers of kidney injury. The identification of 10 mg/kg as the most effective dose provides a valuable basis for future translational studies. Collectively, these findings support disulfiram as a promising repurposed pharmacological candidate for the management of oxidative stress- and fibrosis-associated renal injury and warrant further mechanistic investigation.

6. Strengths and Limitations

The principal strength of this investigation is its integrative, systems-level approach. By concurrently evaluating renal injury and protection across histopathological, molecular, oxidative, and functional tiers, we provide

convergent, multi-faceted validation of disulfiram's renoprotective efficacy. This design mitigates the inherent limitations of single-endpoint analyses and offers a comprehensive pathophysiological narrative.

We acknowledge that our study primarily captures transcriptional and phenotypic endpoints. A recognized challenge in mechanistic studies of fibrosis is the frequent discordance between mRNA and protein levels of key pathway components and extracellular matrix proteins. While our findings support the involvement of the Smad3/Smad7 axis in the observed renoprotective effects of disulfiram, the lack of protein-level validation (e.g., phosphorylated Smad3, TGF-β signaling components, or specific collagen isoforms) represents a limitation. Future studies incorporating targeted protein analyses and spatial localization techniques will be important to further clarify the molecular mechanisms linking transcriptional regulation to attenuation of renal fibrosis.

7. Acknowledgments

The authors thank Babol University of Medical Sciences for its support. We are grateful to our colleagues and technical staff for their essential contributions to this work.

8. Funding

This study was financially supported by the Vice-Chancellery for Research and Technology of Babol University of Medical Sciences.

9. Competing Interests

The authors declare that they have no competing interests.

10. Ethics Approval and Consent to Participate

The study protocol was reviewed and approved by the Ethics Committee of Babol University of Medical Sciences (Approval code: IR.MUBABOL.AEC.1402.028). Our study is a preclinical animal study and not a human clinical trial. Therefore, the registration of a clinical trial number does not apply to this work.

11. Competing Interests

The authors declare that they have no competing interests.

12. AI-Assisted:

During manuscript preparation, AI-assisted language tools (DeepSeek) were used solely to enhance academic writing style and structural clarity. All AI-generated content was rigorously reviewed, edited, and validated by the authors. No AI tools were used in the study conception, design, data generation, analysis, or interpretation. The authors assume full responsibility for the scientific integrity and conclusions of this manuscript.

13. Data Availability Statement:

The datasets generated and/or analyzed during the current study are available from the corresponding author upon reasonable request.

14. References

Agrawal, N., & Gowrishankar, S. (2024). Utility of an Objective Scoring System for Acute Tubular Injury in Renal Allograft Biopsies. *Indian Journal of Transplantation, 18*(4), 374-378. DOI: 10.4103/ijot.ijot_30_24

Awadalla, E. A. (2012). Efficacy of vitamin C against liver and kidney damage induced by paraquat toxicity. *Experimental and toxicologic pathology, 64*(5), 431-434. https://d1wqtxts1xzle7.cloudfront.net/89152099/dx.doi.org/10.1016/j.etp.2010.10.009

Bahramibanan, F., Rad, M. V., Ranjbar, A., Karbasi, A., & Abbasifard, A. (2025). Comparison of oxidative stress status in the kidney tissue of male rats treated with paraquat and nanoparaquat. *Scientific reports, 15*(1), 389. https://doi.org/10.1038/s41598-024-83156-2

Cai, Q., Sun, Z., Xu, S., Jiao, X., Guo, S., Li, Y., . . . Yu, X. (2022). Disulfiram ameliorates ischemia/reperfusion-induced acute kidney injury by suppressing the caspase-11-GSDMD pathway. *Renal Failure, 44*(1), 1170-1182. https://www.tandfonline.com/action/showCitFormats?doi=10.1080/0886022X.2022.2098764

Chen, P.-S., Li, Y.-P., & Ni, H.-F. (2019). Morphology and evaluation of renal fibrosis. *Renal fibrosis: Mechanisms and therapies*, 17-36. https://link.springer.com/series/5584

Chung, A. C., Dong, Y., Yang, W., Zhong, X., Li, R., & Lan, H. Y. (2013). Smad7 suppresses renal fibrosis via altering expression of TGF-β/Smad3-regulated microRNAs. *Molecular Therapy, 21*(2), 388-398. https://doi.org/10.1038/mt.2012.251

de Haan, J. B., Bladier, C., Griffiths, P., Kelner, M., O'Shea, R. D., Cheung, N. S., . . . Zheng, S. S. (1998). Mice with a homozygous null mutation for the most abundant glutathione peroxidase, Gpx1, show increased susceptibility to the oxidative stress-inducing agents paraquat and hydrogen peroxide. *Journal of Biological Chemistry, 273*(35), 22528-22536. https://doi.org/10.1074/jbc.273.35.22528

Dituri, F., Cossu, C., Mancarella, S., & Giannelli, G. (2019). The interactivity between TGFβ and BMP signaling in organogenesis, fibrosis, and cancer. *Cells, 8*(10), 1130. https://doi.org/10.3390/cells8101130

Du, R., Sun, F., Li, K., Qi, J., Zhong, W., Wang, W., . . . Nie, J. (2023). Proteomics Analysis Revealed Smad3 as a Potential Target of the Synergistic Antitumor Activity of Disulfiram and Cisplatin in Ovarian Cancer. *Anti-Cancer Agents in Medicinal Chemistry-Anti-Cancer Agents), 23*(15), 1754-1764. https://doi.org/10.2174/1871520623666230516161200

Gu, Y.-Y., Liu, X.-S., Huang, X.-R., Yu, X.-Q., & Lan, H.-Y. (2020). TGF-β in renal fibrosis: triumphs and challenges. *Future Medicinal Chemistry, 12*(9), 853-866. https://doi.org/10.4155/fmc-2020-0005

Gu, Y.-Y., Liu, X.-S., & Lan, H.-Y. (2024). Therapeutic potential for renal fibrosis by targeting Smad3-dependent noncoding RNAs. *Molecular Therapy, 32*(2), 313-324. https://doi.org/10.1016/j.ymthe.2023.12.009

Guo, W., Chen, S., Li, C., Xu, J., & Wang, L. (2022). Application of disulfiram and its metabolites in treatment of inflammatory disorders. *Frontiers in pharmacology, 12*, 795078. https://doi.org/10.3389/fphar.2021.795078

Hamidi, N., Feizi, F., Azadmehr, A., Zabihi, E., Khafri, S., Zarei-Behjani, Z., & Babazadeh, Z. (2023). Disulfiram ameliorates bleomycin induced pulmonary inflammation and fibrosis in rats. *Biotechnic & Histochemistry, 98*(8), 584-592. https://doi.org/10.1080/10520295.2023.2261367

Hasan, M. I., Das, S. K., & Chowdhury, E. H. (2021). A better and copacetic protocol for histopathological slide preparation using H&E stain: A review. *J. Fish, 2*, 57-67.

Hassan, I., Ebaid, H., Alhazza, I. M., Al-Tamimi, J., Aman, S., & Abdel-Mageed, A. M. (2019). Copper Mediates Anti-Inflammatory and Antifibrotic Activity of Gleevec in Hepatocellular Carcinoma-Induced Male Rats. *Canadian Journal of Gastroenterology and Hepatology, 2019*(1), 9897315. https://doi.org/10.1155/2019/9897315

Hassan, I., Ebaid, H., Alhazza, I. M., Al-Tamimi, J., & Rady, A. M. (2023). Disulfiram enhances the antineoplastic activity and sensitivity of murine hepatocellular carcinoma to 5-FU via redox management. *Pharmaceuticals, 16*(2), 169. https://doi.org/10.3390/ph16020169

Hong, Q., Kim, H., Cai, G.-Y., Chen, X.-M., He, J. C., & Lee, K. (2025). Modulation of TGF-β signaling new approaches toward kidney disease and fibrosis therapy. *International Journal of Biological Sciences, 21*(4), 1649. https://doi.org/10.7150/ijbs.101548

Hoshino, J., Mise, K., Ueno, T., Imafuku, A., Kawada, M., Sumida, K., . . . Hayami, N. (2015). A pathological scoring system to predict renal outcome in diabetic nephropathy. *American Journal of Nephrology, 41*(4-5), 337-344. https://doi.org/10.1159/000431333

Huang, R., Fu, P., & Ma, L. (2023). Kidney fibrosis: from mechanisms to therapeutic medicines. *Signal transduction and targeted therapy, 8*(1), 129. https://doi.org/10.1159/000431333

Isha, I. T., Alam, Z. N., Shaha, B. K., Bari, M. S., Bari, M. Z. J., & Chowdhury, F. R. (2018). Paraquat induced acute kidney injury and lung fibrosis: a case report from Bangladesh. *BMC research notes, 11*(1), 344. https://doi.org/10.1186/s13104-018-3425-3

Jiang, H., Zhao, Y., Tang, H., Duan, S., Li, M., Yang, X., . . . Zhao, W. (2021). Tetraethylthiuram disulphide alleviates pulmonary fibrosis through modulating transforming growth factor-β signalling. *Pharmacological Research, 174*, 105923. https://doi.org/10.1016/j.phrs.2021.105923

Jiao, H., Zhang, M., Chen, L., & Zhang, Z. (2025). Traditional Chinese Medicine targeting the TGF-β/Smad signaling pathway as a potential therapeutic strategy for renal fibrosis. *Frontiers in pharmacology, 16*, 1513329. https://doi.org/10.3389/fphar.2025.1513329

Jing, H., Gao, Y., Jing, L., Yang, H., & Liu, S. (2025). Recent advances in therapeutic use of transforming growth factor-beta inhibitors in cancer and fibrosis. *Frontiers in Oncology, 15*, 1489701. doi: 10.3389/fonc.2025.1489701

Juan, Y.-H., Yu, Y.-L., Tsai, Y.-P., Lee, C.-C., Chen, Y.-S., Ting, Y.-H., . . . Hsieh, Y.-H. (2023). Alpha-mangostin alleviate renal interstitial fibrosis via suppression of TGF-β1/Smad/ERK signaling axis in vitro and in vivo. *Biochemical Pharmacology, 218*, 115935. https://doi.org/10.1016/j.bcp.2023.115935

Kalantar-Zadeh, K., Jafar, T. H., Nitsch, D., Neuen, B. L., & Perkovic, V. (2021). Chronic kidney disease. *The lancet, 398*(10302), 786-802. DOI: 10.1016/S0140-6736(21)00519-5

Karimzadeh, F., Daraei, A., Zabihi-Neyshaburi, E., Feizi, F., Ranaee, M., Khafri, S., . . . Babazadeh, Z. (2025). Repurposing disulfiram: targeting Zeb1 to attenuate paraquat-induced pulmonary fibrosis in rats. *Journal of Molecular Histology, 56*(5), 318. https://doi.org/10.1007/s10735-025-10613-1

Li, Y., Wang, L. H., Zhang, H. T., Wang, Y. T., Liu, S., Zhou, W. L., . . . Yang, J. Y. (2018). Disulfiram combined with copper inhibits metastasis and epithelial–mesenchymal transition in hepatocellular carcinoma through the NF-κB and TGF-β pathways. *Journal of cellular and molecular medicine, 22*(1), 439-451. https://doi.org/10.1111/jcmm.13334

Mallone, F., Costi, R., Marenco, M., Plateroti, R., Minni, A., Attanasio, G., . . . Lambiase, A. (2021). Understanding drivers of ocular fibrosis: current and future therapeutic perspectives. *International journal of molecular sciences, 22*(21), 11748. https://doi.org/10.3390/ijms222111748

McGwin Jr, G., & Griffin, R. L. (2022). An ecological study regarding the association between paraquat exposure and end stage renal disease. *Environmental Health, 21*(1), 127.

Meng, X.-M., Chung, A. C., & Lan, H. Y. (2013). Role of the TGF-β/BMP-7/Smad pathways in renal diseases. *Clinical science, 124*(4), 243-254. https://doi.org/10.1186/s12940-022-00946-9

Nouri, A., Ghorbani, M., & Shahriary, A. (2025). Mitigation of renal toxicity induced by paraquat using ferulic acid: Role of inflammatory pathways. *Avicenna Journal of Phytomedicine, 15*(6). doi: 10.22038/ajp.2025.26035

Okabe, Y., Toda, E., Urushiyama, H., Terashima, Y., Kunugi, S., Kajimoto, Y., . . . Yamauchi, Y. (2024). Antifibrotic effect of disulfiram on bleomycin-induced lung fibrosis in mice and its impact on macrophage infiltration. *Scientific reports, 14*(1), 23653. https://doi.org/10.1038/s41598-024-71770-z

Pei, J., Pan, X., Wei, G., & Hua, Y. (2023). Research progress of glutathione peroxidase family (GPX) in redoxidation. *Frontiers in pharmacology, 14*, 1147414. https://doi.org/10.3389/fphar.2023.1147414

Prayaga, A. K., Anuradha, S., Manjusha, Y., Uppin, M., Rapur, R., & Murthy, K. D. (2011). Morphologic evaluation of renal function using semi-quantitative method in primary nonproliferative glomerular diseases. *Indian Journal of Pathology and Microbiology, 54*(1), 42-46. DOI: 10.4103/0377-4929.77322

Rieder, F., Nagy, L. E., Maher, T. M., Distler, J. H., Kramann, R., Hinz, B., & Prunotto, M. (2025). Fibrosis: cross-organ biology and pathways to development of innovative drugs. *Nature Reviews Drug Discovery*, 1-27.

Saifi, M. A., & Godugu, C. (2022). Copper chelation therapy inhibits renal fibrosis by modulating copper transport proteins. *BioFactors, 48*(4), 934-945. https://doi.org/10.1002/biof.1837

Saifi, M. A., Shaikh, A. S., Kaki, V. R., & Godugu, C. (2022). Disulfiram prevents collagen crosslinking and inhibits renal fibrosis by inhibiting lysyl oxidase enzymes. *Journal of Cellular Physiology, 237*(5), 2516-2527. https://doi.org/10.1002/jcp.30717

Saleh, S. M., Mahmoud, A. B., Al-Salahy, M. B., & Mohamed Moustafa, F. A. (2023). Morphological, immunohistochemical, and biochemical study on the ameliorative effect of gallic acid against bisphenol A-induced nephrotoxicity in male albino rats. *Scientific reports, 13*(1), 1732. https://doi.org/10.1038/s41598-023-28860-1

Shadnia, S., Ebadollahi-Natanzi, A., Ahmadzadeh, S., Karami-Mohajeri, S., Pourshojaei, Y., & Rahimi, H. R. (2018). Delayed death following paraquat poisoning: three case reports and a literature review. *Toxicology Research, 7*(5), 745-753.

Sittipunt, C. (2005). Paraquat poisoning. *Respiratory care, 50*(3), 383-385. http://www.liebertpub.com/

Sridharan, D., Pracha, N., Dougherty, J. A., Akhtar, A., Alvi, S. B., & Khan, M. (2022). A one-stop protocol to assess myocardial fibrosis in frozen and paraffin sections. *Methods and Protocols, 5*(1), 13. https://doi.org/10.3390/mps5010013

Subbiah, R., & Tiwari, R. R. (2021). The herbicide paraquat-induced molecular mechanisms in the development of acute lung injury and lung fibrosis. *Critical reviews in Toxicology, 51*(1), 36-64. https://doi.org/10.1080/10408444.2020.1864721

Sule, R. O., Condon, L., & Gomes, A. V. (2022). A common feature of pesticides: oxidative stress—the role of oxidative stress in pesticide-induced toxicity. *Oxidative medicine and cellular longevity, 2022*(1), 5563759. https://doi.org/10.1155/2022/5563759

Tayeb, F. J., Felemban, M. F., Adnan Ashour, A., & Shafie, A. (2024). Paraquat-induced toxicities: epidemiological insights and advances in colorimetric and Fluorimetric detection methods. *Critical Reviews in Analytical Chemistry*, 1-31. https://doi.org/10.1080/10408347.2024.2433005

Toda, E., Sawada, A., Takeuchi, K., Wakamatsu, K., Ishikawa, A., Kuwahara, N., . . . Makino, K. (2022). Inhibition of the chemokine signal regulator FROUNT by disulfiram ameliorates crescentic glomerulonephritis. *Kidney International, 102*(6), 1276-1290. https://doi.org/10.1016/j.kint.2022.07.031

Wal, A., Rasheed, A., Wal, P., Bhise, M. R., Parmar, M., Nathiya, D., . . . Gasmi, A. (2025). The Therapeutic Potential of TGF-β as a Target for Multiple Chronic Diseases: A Comprehensive Review of Pharmacologically Approved Drugs and Investigational Agents. *Current Signal Transduction Therapy, 20*(2), E15743624339476. https://doi.org/10.2174/0115743624339476250212114656

Wang, J., Jiang, X., Lu, G., Zhou, J., Kang, J., & Zhang, J.-s. (2020). Identify the early predictor of mortality in patients with acute paraquat poisoning. *BioMed research international, 2020*(1), 8894180. https://doi.org/10.1155/2020/8894180

Wang, Y., Ping, Z., Gao, H., Liu, Z., Xv, Q., Jiang, X., & Yu, W. (2024). LYC inhibits the AKT signaling pathway to activate autophagy and ameliorate TGFB-induced renal fibrosis. *Autophagy, 20*(5), 1114-1133. https://doi.org/10.1080/15548627.2023.2287930

Wang, Z., Yang, J., Tu, M., Zhang, R., Ma, Y., Jin, H., . . . Wang, Z. (2024). Integrin-β1 aggravates paraquat-induced pulmonary fibrosis by activation of FAK/ERK1/2 pathway depending on fibrotic ECM. *International Immunopharmacology, 141*, 112947. https://doi.org/10.1016/j.intimp.2024.112947

Wu, W., Wang, X., Yu, X., & Lan, H.-Y. (2022). Smad3 signatures in renal inflammation and fibrosis. *International Journal of Biological Sciences, 18*(7), 2795. doi: 10.7150/ijbs.71595

Xiong, W., Li, J., Mao, X., Qian, Z., Tian, A., Peng, X., . . . Li, Z. (2025). Disulfiram alleviates immune-mediated liver injury by inhibiting pyroptosis in hepatocytes through the NF-κB pathway. *European Journal of Pharmacology, 992*, 177352. https://doi.org/10.1016/j.ejphar.2025.177352

Yang, X.-M., Wu, Z., Wang, X., Zhou, Y., Zhu, L., Li, D., . . . Ma, X. (2022). Disulfiram inhibits liver fibrosis in rats by suppressing hepatic stellate cell activation and viability. *BMC Pharmacology and Toxicology, 23*(1), 54. https://doi.org/10.1186/s40360-022-00583-5

Yu, X.-Y., Sun, Q., Zhang, Y.-M., Zou, L., & Zhao, Y.-Y. (2022). TGF-β/Smad signaling pathway in tubulointerstitial fibrosis. *Frontiers in pharmacology, 13*, 860588. https://doi.org/10.3389/fphar.2022.860588

Zakout, Y. M.-A., Abdellah, M. A., Abdallah, M. A., & Batran, S. A. (2024). Optimization of PAS stain and similar Schiff's based methods for glycogen demonstration in liver tissue. *Histochemistry and Cell Biology, 161*(4), 359-364. DOI: 10.1007/s00418-023-02261-x

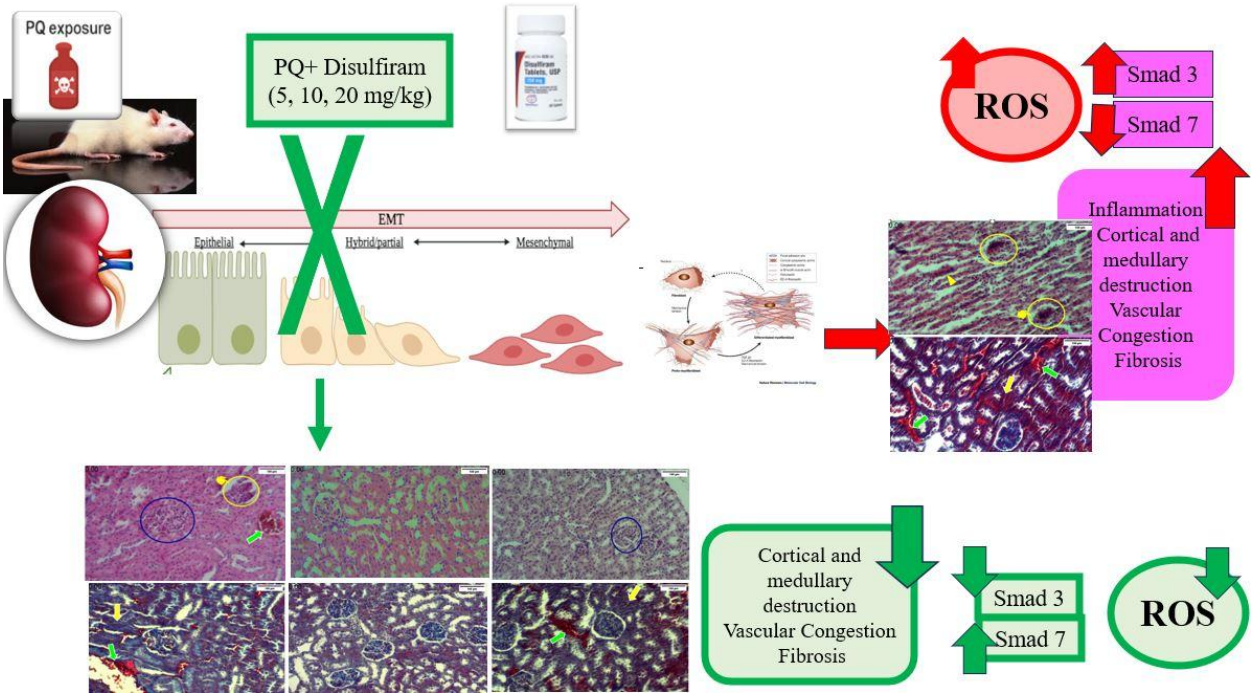
Zhang, H., Yang, H., Liu, X.-m., Ying, J., Zu, T., Jiang, J., . . . Jin, J. (2024). Targeted inhibition of transforming growth factor-β type I receptor by AZ12601011 improves paraquat poisoning-induced multiple organ fibrosis. *Pesticide Biochemistry and Physiology, 200*, 105831. https://doi.org/10.1016/j.pestbp.2024.105831

Zhanga, Y., & Wub, X. (2025). Targeting TGF-β/Smad in Chronic Kidney Disease Fibrosis: Mechanisms and TCM Therapeutics. *International Journal of Frontiers in Medicine, 7*(2). DOI: 10.25236/IJFM.2025.070212

Zou, T., He, P., Cao, J., & Li, Z. (2015). Determination of paraquat in vegetables using HPLC–MS-MS. *Journal of Chromatographic Science, 53*(2), 204-209. https://doi.org/10.1093/chromsci/bmu041

Figure ligand

Graphical abstract



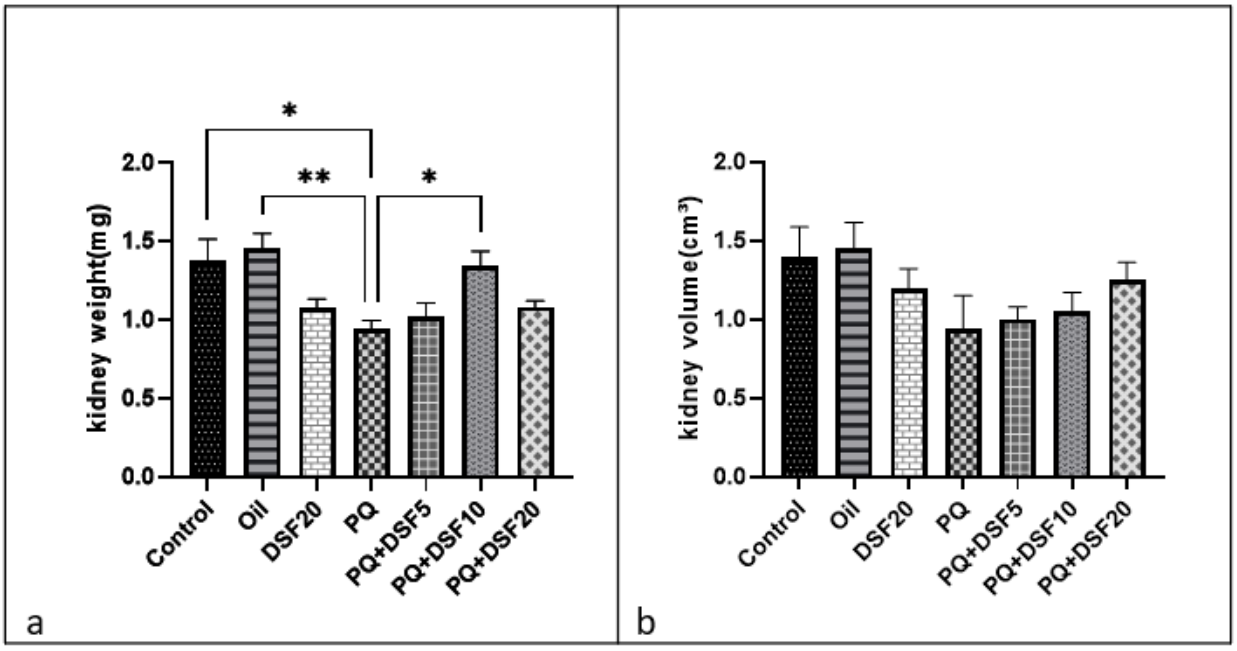


Figure 1. Kidney morphometric analysis.

(a) Mean ± SEM kidney weight and (b) kidney volume across experimental groups. Data are presented as mean ± SEM (n = 5 per group). Statistical significance was determined by one-way ANOVA with Tukey's post-hoc multiple comparisons test. Significant pairwise differences are indicated on the graphs (*P ≤ 0.05, **P ≤ 0.01, ***P ≤ 0.001, ****P ≤ 0.0001).

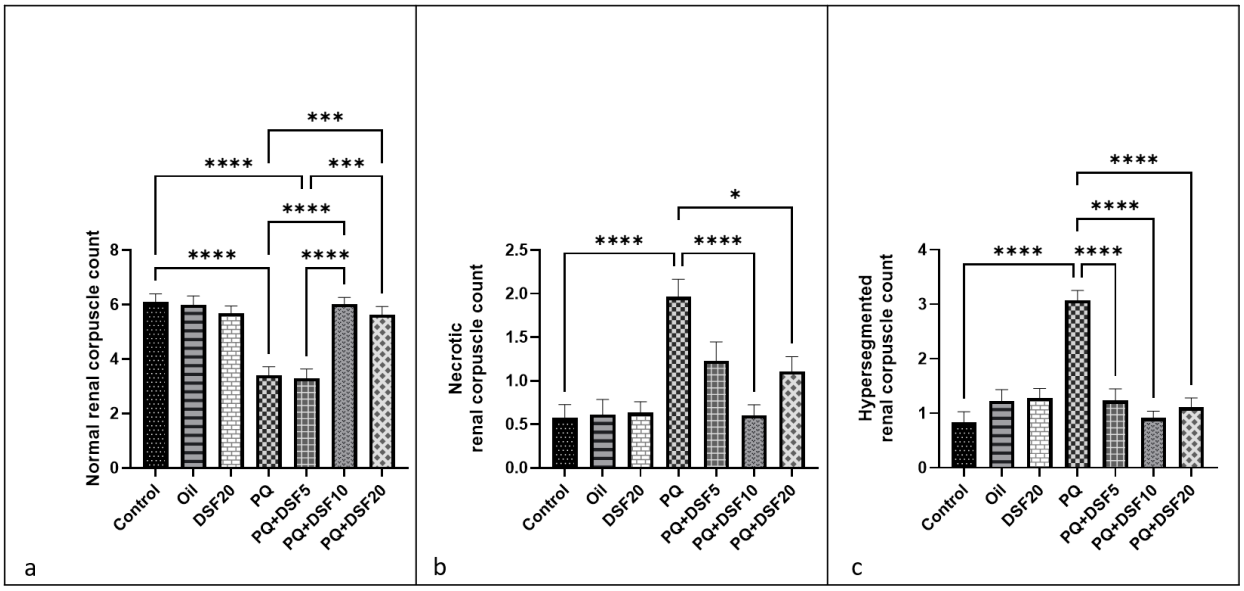


Figure 2. Quantification of intact, necrotic, and hyper-segmented renal corpuscles across experimental groups in 18× microscopic fields.

a) Normal renal corpuscle count, b) Necrotic renal corpuscle count, c) hypersegmented renal corpuscle count. Statistical analysis was performed using the Kruskal–Wallis test, followed by Dunn's post-hoc test for inter-group comparisons. Significance levels are indicated as follows: * $P \leq 0.05$, ** $P \leq 0.01$, *** $P \leq 0.001$, **** $P \leq 0.0001$.

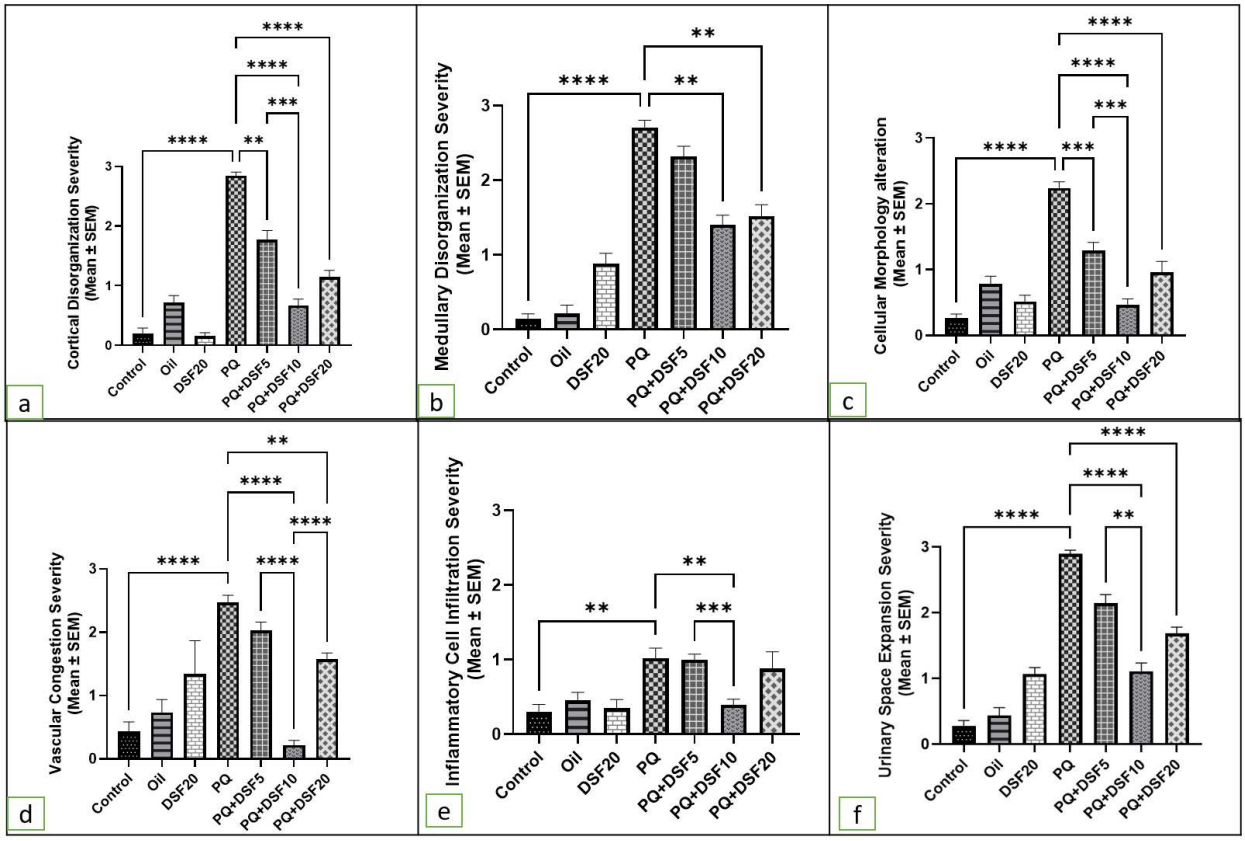


Figure 3: Semi-quantitative histopathological scoring of cortical and medullary alteration across experimental groups.

a). cortical disorganization, b) medullary disorganization, c) cellular morphology disruption, d) vascular congestion, e) inflammatory cell infiltration, f) urinary expansion. Statistical analysis was performed using the Kruskal–Wallis test, followed by Dunn's post hoc test for intergroup comparisons. Significance levels are indicated as follows: * $P \leq 0.05$, ** $P \leq 0.01$, *** $P \leq 0.001$, **** $P \leq 0.0001$.

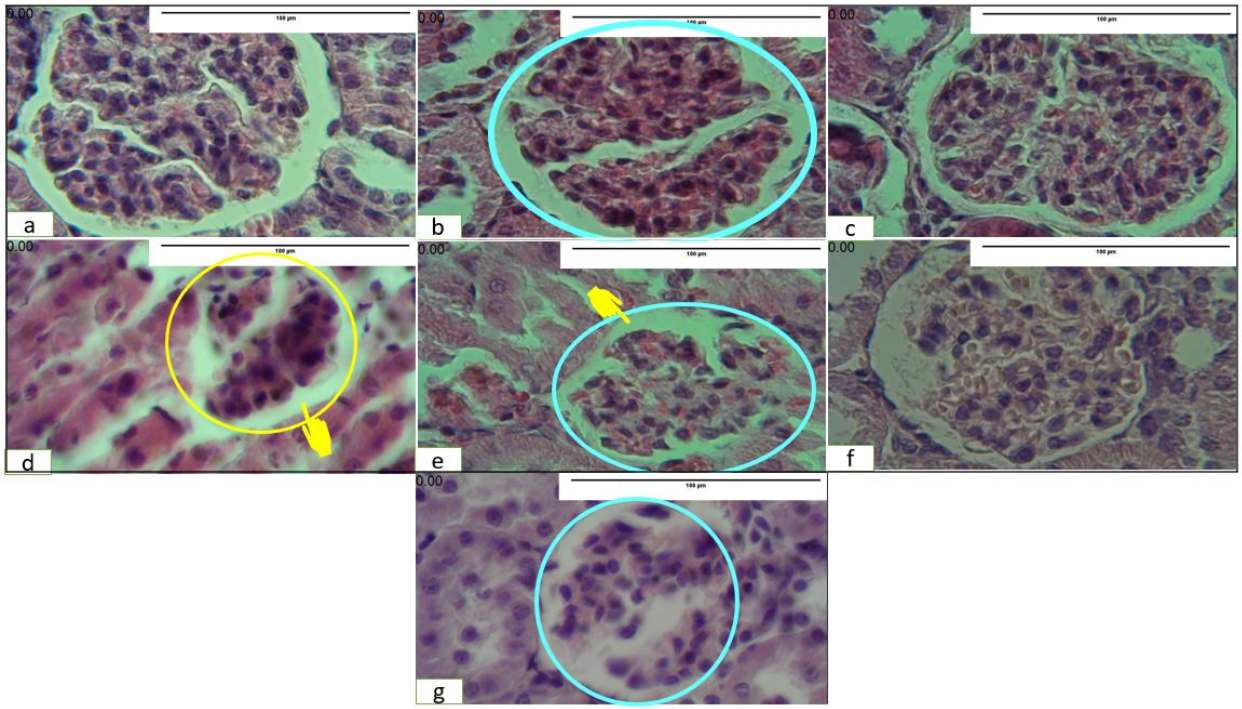


Figure 4. Renal cortical histology (H&E).

Groups: a: Control; b: Vehicle (oil); c: DSF20 alone; d: PQ; e: PQ+DSF5; f: PQ+DSF10; g: PQ+DSF20.

Normal architecture is seen in control/vehicle groups. Annotations: hyper-segmented glomeruli (blue circles), necrotic glomeruli (yellow circles), Bowman's space expansion (hand symbol), . Scale bar = 100 μm.

(a-g) magnification: 40× with 4.5× camera zoom)

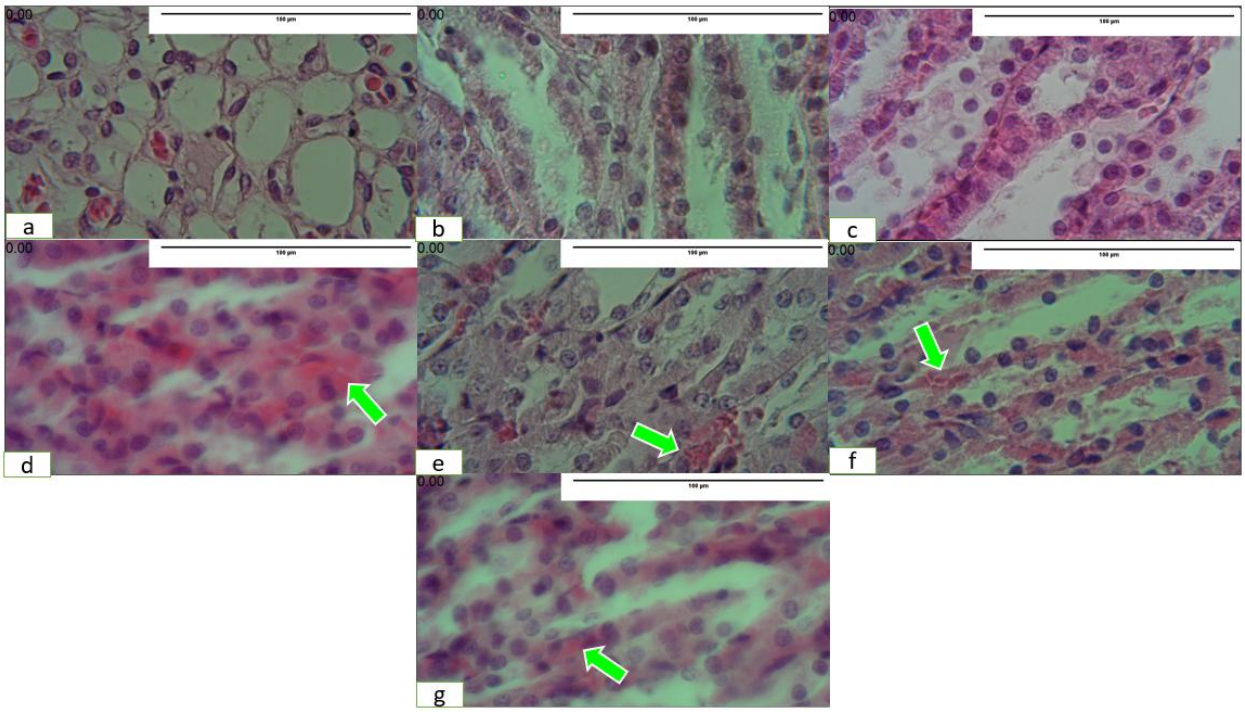


Figure 5. Renal medullary histology (H&E).

Groups: a: Control; b: Oil; c: DSF20; d: PQ; e: PQ+DSF5; f: PQ+DSF10; g: PQ+DSF20.

Vascular congestion (green arrows) is shown. Scale bar = 100 μm. Magnification: 40× (a-g; with 4.5× camera zoom).

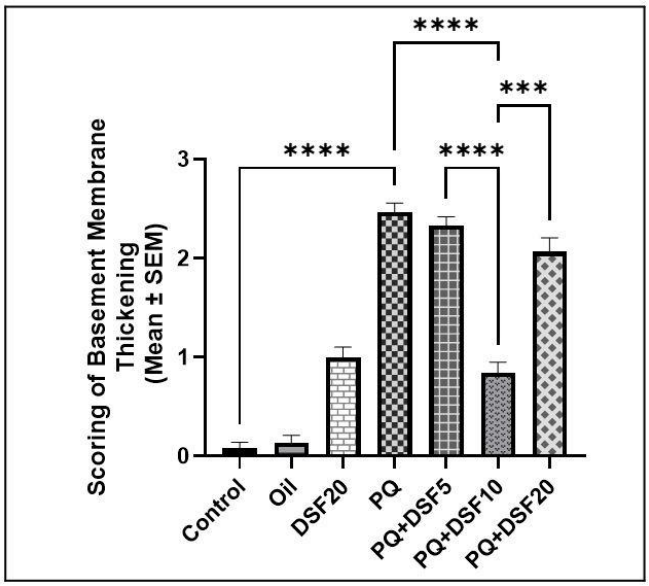


Figure 6: Semi-quantitative Basement membrane thickness scoring across experimental groups.

Statistical analysis was performed using the Kruskal–Wallis test, followed by Dunn's post hoc test for intergroup comparisons. Significance levels are indicated as follows: * $P \leq 0.05$, ** $P \leq 0.01$, *** $P \leq 0.001$, **** $P \leq 0.0001$.

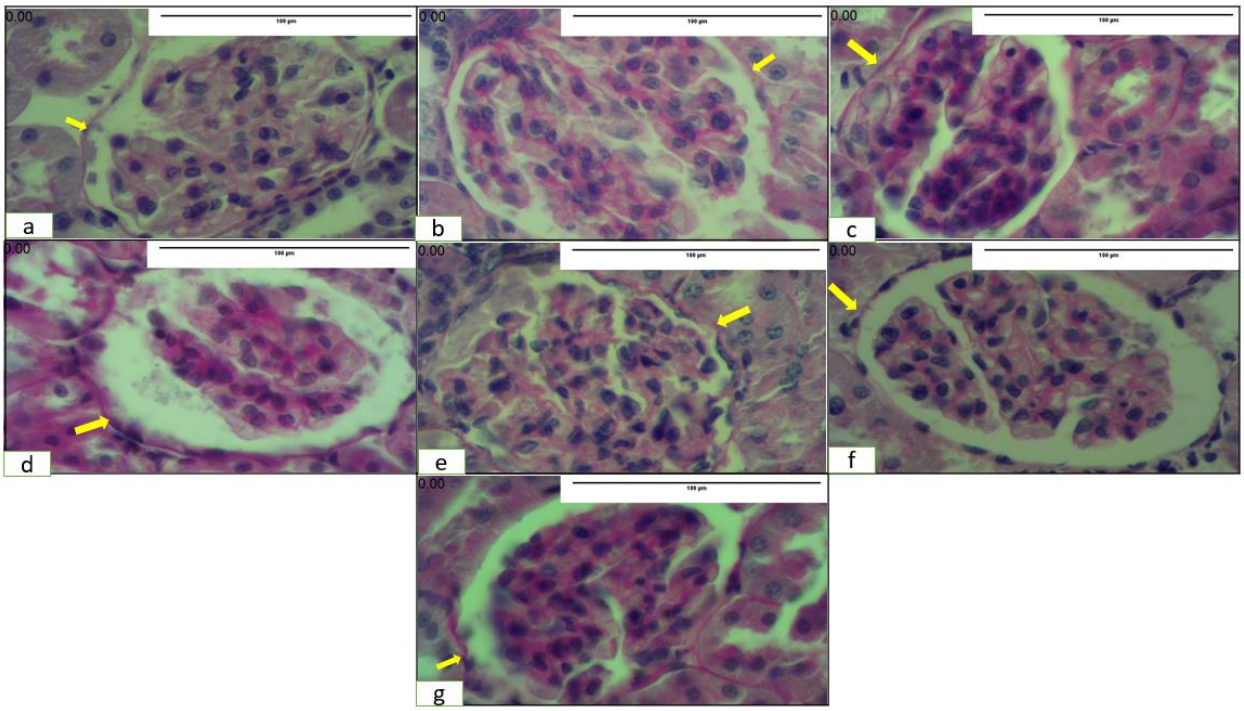


Figure 7. Renal PAS staining.

Groups: a: Control; b: Oil; c: DSF20; d: PQ; e: PQ+DSF5; f: PQ+DSF10; g: PQ+DSF20.

Yellow arrows indicate glomerular basement membrane thickening. Scale bar = 100 μm.

Magnification: 40× (a-g with 4.5× camera zoom).

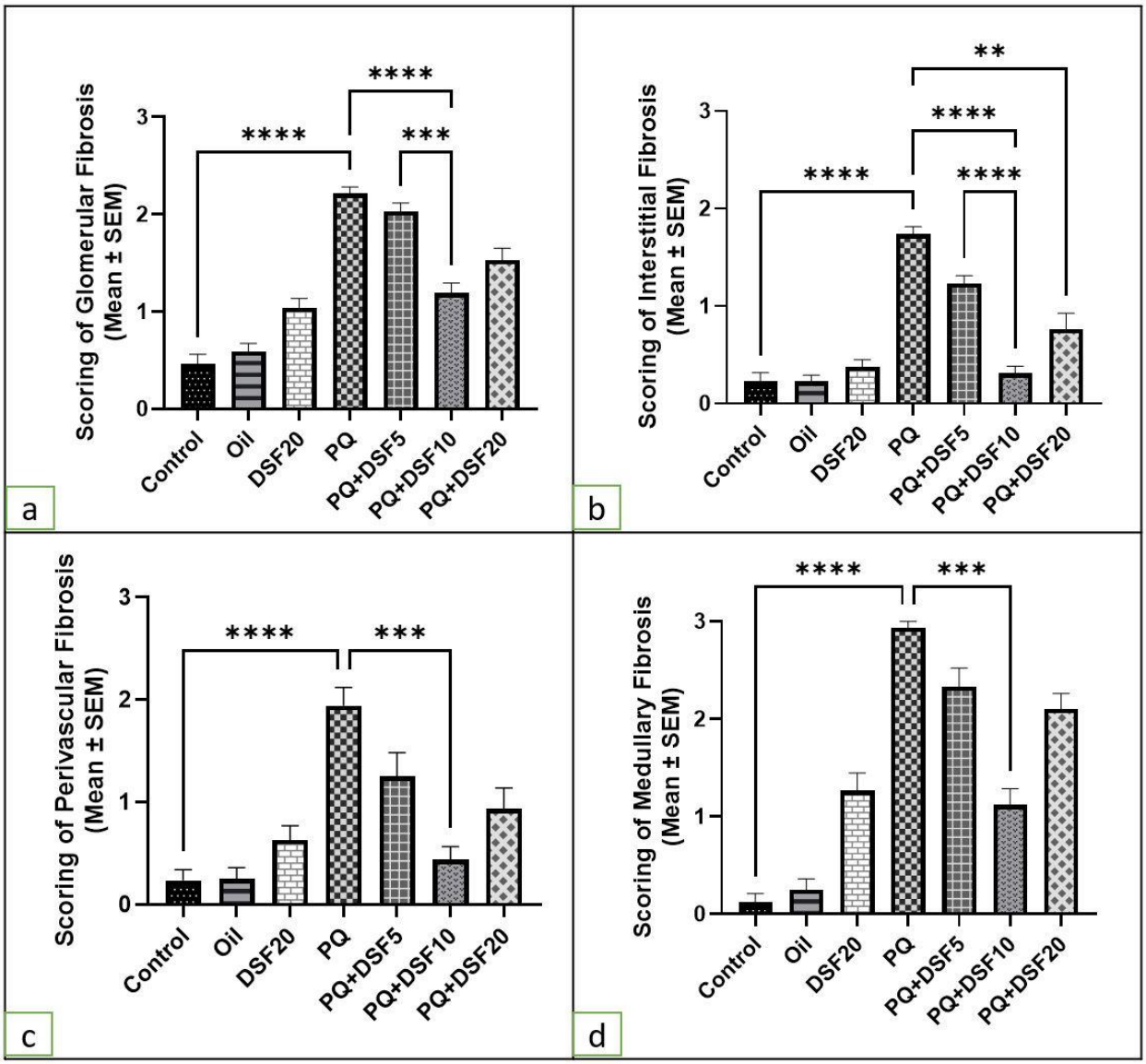


Figure 8: Semi-quantitative fibrotic scoring across experimental groups.

a). Scoring of glomerular fibrosis, b) Scoring of interstitial fibrosis, c) Scoring of perivascular fibrosis, and d) Scoring of medullary fibrosis. Statistical analysis was performed using the Kruskal–Wallis test, followed by Dunn's post hoc test for intergroup comparisons. Significance levels are indicated as follows: * $P \leq 0.05$, ** $P \leq 0.01$, *** $P \leq 0.001$, **** $P \leq 0.0001$.

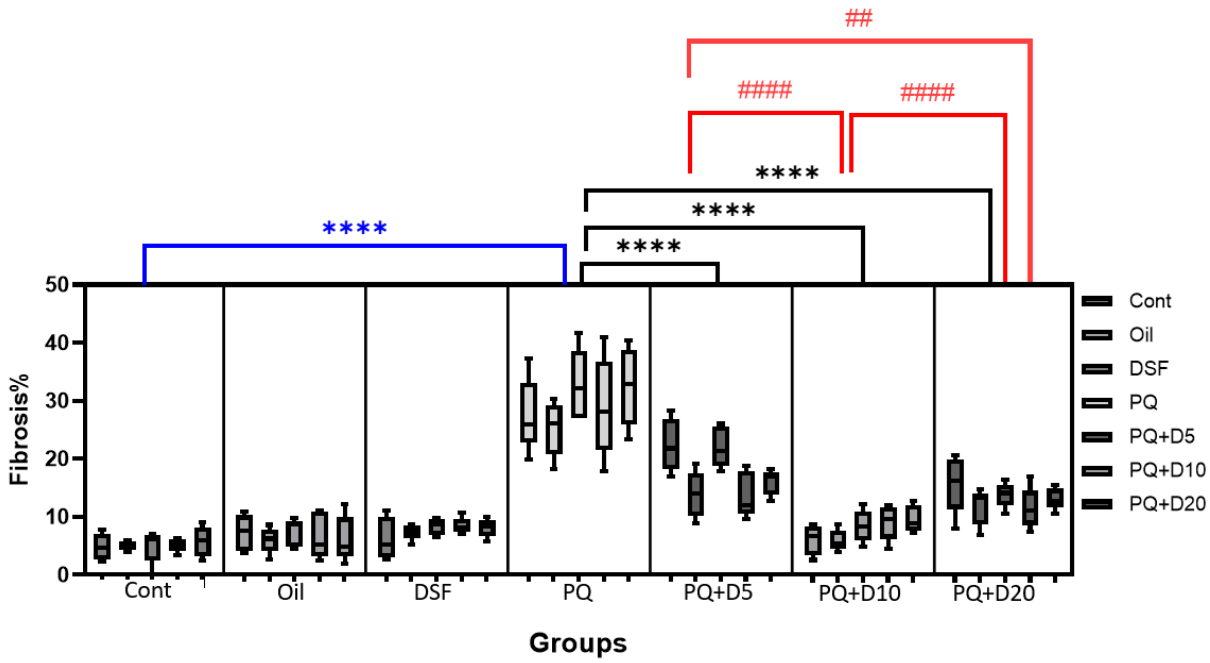


Figure 9. Quantitative analysis of renal interstitial fibrosis in experimental groups.

Renal fibrosis was quantified histomorphometrically using Masson's trichrome staining and expressed as the percentage of collagen-positive area (% Fibrosis). Data are presented as box-and-whisker plots (minimum to maximum; n=5 animals per group). Experimental groups: Cont (control), Oil (vehicle control, received oil solvent), DSF (disulfiram 20 mg/kg alone), PQ (paraquat), PQ+D5 (paraquat + disulfiram 5 mg/kg), PQ+D10 (paraquat + disulfiram 10 mg/kg), PQ+D20 (paraquat + disulfiram 20 mg/kg). Statistical analysis was performed using nested one-way ANOVA followed by appropriate post hoc tests for multiple comparisons. Significance levels: ****, $P \leq 0.0001$ versus control group. ##, $P \leq 0.01$; ####, $P \leq 0.0001$ between indicated experimental groups.

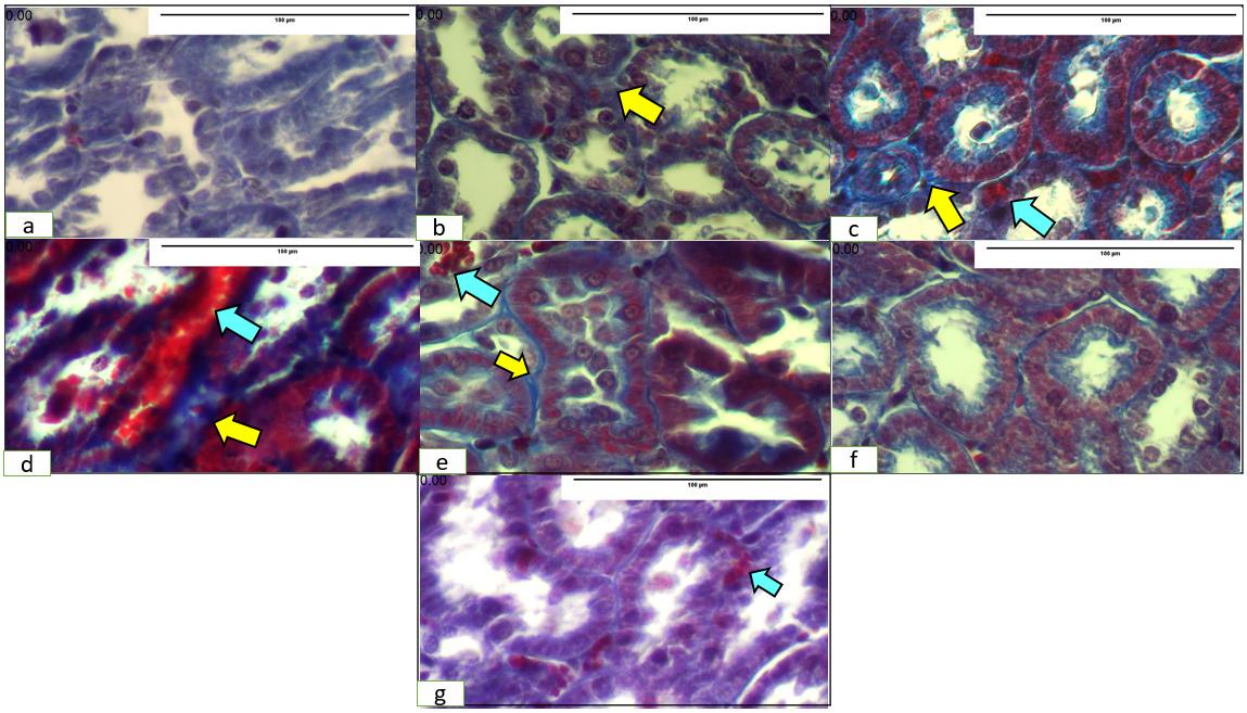


Figure 10. Renal fibrosis (Mallory's trichrome).

Groups: a: Control; b: Oil; c: DSF20; d: PQ; e: PQ+DSF5; f: PQ+DSF10; g: PQ+DSF20.

Yellow arrows: fibrotic area (collagen accumulation). Blue arrows: congested vessels. These features were more severe in the PQ group and attenuated with co-treatment with disulfiram. Scale bar = 100 μm.

Magnification: 40× (a-g; with 4.5× camera zoom).

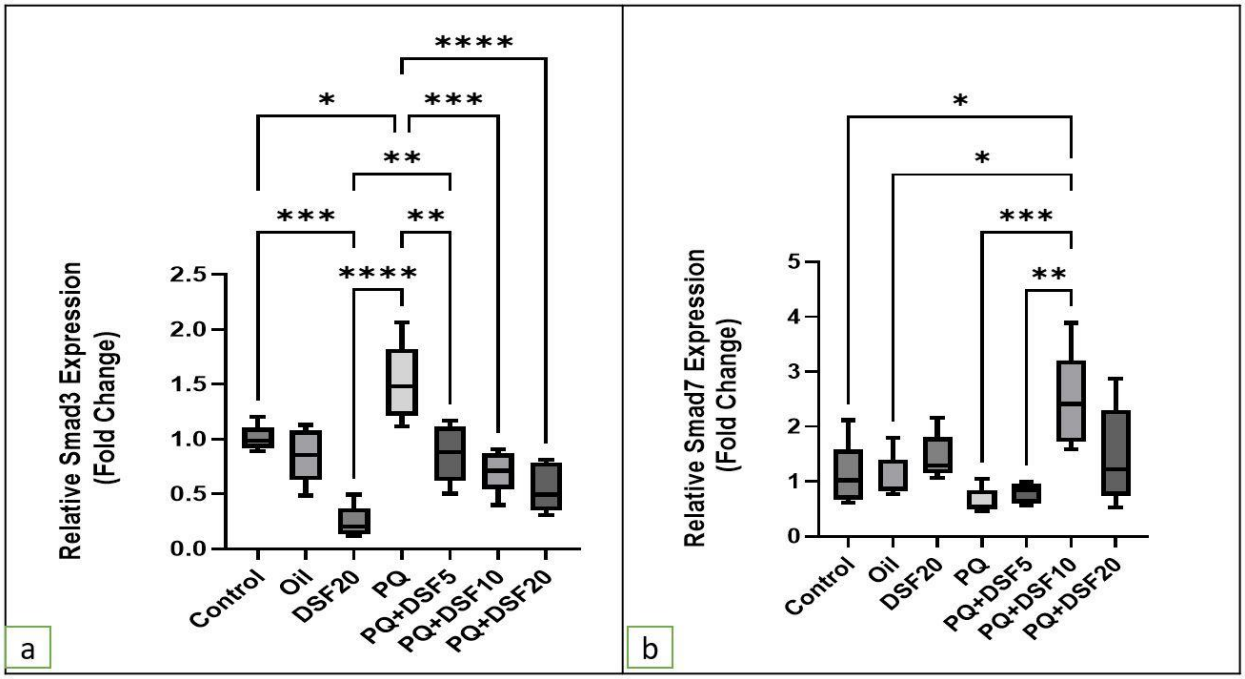


Figure 11: Smad3 and Smad7 mRNA expression levels in renal tissue.

Relative *Smad3* (a) and Smad7 (b) gene expression was analyzed by quantitative RT-PCR using the 2^(-ΔΔCt) method, normalized to *Gapdh* as the endogenous control. Data are expressed as mean fold change ± SEM (n = 5 per group). Statistical analysis was performed using one-way ANOVA followed by Tukey's multiple comparisons test. Significant pairwise differences are denoted on the graph (*p < 0.05, **p < 0.01, ***p < 0.001, ****p < 0.0001).

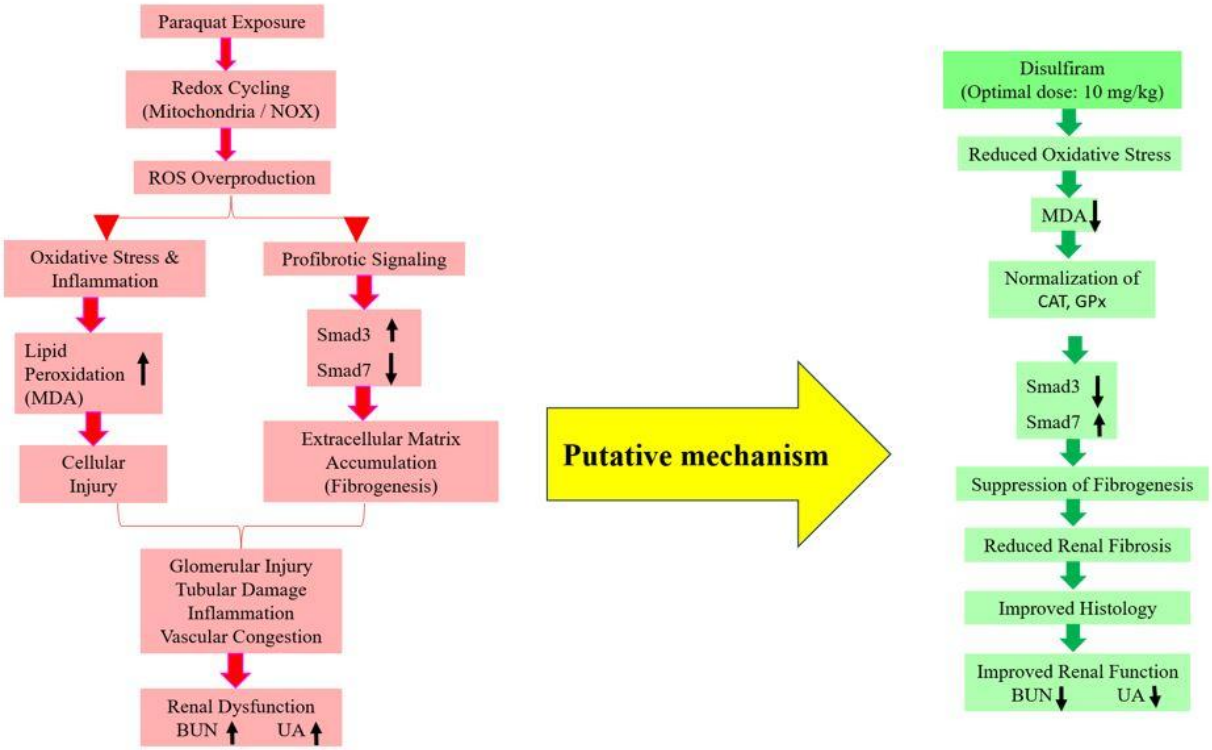


Figure 12: Proposed mechanism of disulfiram-mediated renoprotection against paraquat-induced renal fibrosis. Paraquat-induced redox cycling promotes ROS generation, oxidative stress, inflammation, and activation of profibrotic signaling pathways associated with increased Smad3 and decreased Smad7 expression. These changes contribute to extracellular matrix accumulation, renal fibrosis, and functional impairment. Disulfiram mitigates oxidative stress, normalizes antioxidant defense, modulates Smad3/Smad7 expression, and attenuates renal fibrosis and dysfunction. The mechanism shown is proposed based on the findings of the present study.

1 **Tables**

2 Table 1: Effects of disulfiram co-treatment on oxidative stress markers in paraquat-induced nephrotoxicity.

Stress oxidative marker		**Cont**	**Oil**	**DSF20**	**PQ**	**PQ+ DSF5**	**PQ+ DSF10**	**PQ+ DSF20**	**P value PQ and Treat**
MDA	Mea± SEM	4.56±0.15	4.65± 0.21	5.96± 0.45	6.66± 0.45	4.98± 0.3	4.44± 0.31	6.09± 0.4	**PQ vs. PQ+DSF5** P=0.0284* **PQ vs. PQ+DSF10** P=0.0018** **PQ vs. PQ+DSF20** P=0.8976 ns
	Median	4.551	4.654	5.962	6.816	4.776	4.604	6.201	
	IQR	(4.23, 4.88)	(4.174, 5.145)	(5.071, 6.853)	(5.769, 7.496)	(4.371, 5.701)	(3.769, 5.034)	(5.247, 6.877)	
GPx	Mea± SEM	21.17±2.8	42.48± 4.19	38.8± 5.06	48.71± 5.34	17.72± 2.77	36.18±2.53	59.59±2.55	**PQ vs. PQ+DSF5** P<0.0001**** **PQ vs. PQ+DSF10** P= 0.2605 ns **PQ vs. PQ+DSF20** P= 0.4178 ns
	Median	22.02	45.95	38.45	48.7	15.95	34.12	60.59	
	IQR	(15.97, 25.95)	(32.46, 50.77)	(29.16, 48.63)	(38.09, 59.34)	(12.69, 23.64)	(31.75, 41.63)	(54.43, 64.25)	
CAT	Mea± SEM	87.13±6.52	137.1± 8.21	290.5± 20.55	209.4± 6.84	225.1± 17.68	158.2±10.99	396.3±28.51	**PQ vs. PQ+DSF5** P=0.9922 ns
	Median	85.00	138.3	315.0	211.7	225.0	171.7	371.0	

	IQR	(73.3, 102)	(120.8, 152.8)	(242.5, 326.3)	(193.7, 224)	(185.8, 264.5)	(131.7, 178)	(346.7, 458.7)	**PQ vs. PQ+DSF10** P= 0.3065 ns **PQ vs. PQ+DSF20** P<0.0001****

Values represent mean ± SEM for MDA level, GPx activity, and CAT activity in renal tissue homogenates (n=5 animals per group). Cont, control; Oil, (vehicle); DSF20, disulfiram 20 mg/kg alone; PQ, paraquat 1.5 mg/kg; PQ+DSF5, PQ + disulfiram 5 mg/kg; PQ+DSF10, PQ + disulfiram 10 mg/kg; PQ+DSF20, PQ + disulfiram 20 mg/kg. Statistical analysis: one-way ANOVA with Tukey's multiple comparisons test. *P < 0.05, **P < 0.01, ***P < 0.001

1 Table 2: Statistical analysis of Renal function biomarker in renal Tissue among Treated groups

Renal Function Biomarker		**Cont**	**Oil**	**DSF20**	**PQ**	**PQ+ DSF5**	**PQ+ DSF10**	**PQ+ DSF20**	**P value PQ and Treat**
BUN	Mea± SEM	19.4± 0.24	19.6± 0.24	21.2± 0.58	34.4± 4.17	20.4± 1.28	19± 0.44	24.6± 0.6	**PQ vs. PQ+DSF5** P<0.0001****
	Median	19	20	21	36	22	19	24	
	IQR	(19,20)	(19, 20)	(20,22.5)	(26,42)	(17.5, 22.5)	(18, 20)	(24, 25.5)	**PQ vs. PQ+DSF10** P<0.0001**** **PQ vs. PQ+DSF20** P=0.0055 **
CR	Mea±SEM	0.64± 0.02	0.6± 0	0.64± 0.02	0.62± 02	0.6± 0	0.62± 0.02	0.64± 0.02	**PQ vs. PQ+DSF5** P>0.9999 ns
	Median	0.6	0.6	0.6	0.6	0.6	0.6	0.6	
	IQR	(0.6, 0.7)	(0.6, 0.6)	(0.6, 0.7)	(0.6, 0.65)	(0.6, 0.6)	(0.6, 0.65)	(0.6, 0.7)	**PQ vs. PQ+DSF10** P>0.9999 ns **PQ vs. PQ+DSF20** P>0.9999 ns
UA	Mea± SEM	87.13± 6.52	137.1 ±8.21	290.5± 20.55	209.4± 6.84	225.1± 17.68	396.3± 28.51	158.2± 10.99	**PQ vs. PQ+DSF5** P<0.0001****
	Median	0.9	0.9	0.6	1.8	0.7	0.6	1.6	

	IQR	(0.8, 1.2)	(0.85, 1.62)	(0.6, 1.15)	(1.3, 1.85)	(0.55, 0.75)	(0.5, 0.75)	(1.5, 1.8)	**PQ vs. PQ+DSF10** P<0.0001**** **PQ vs. PQ+DSF20** P>0.9999 ns

1 Values represent mean ± SEM for BUN, Creatin, and UA level (n=5 animals per group). Cont, control; Oil,

2 (vehicle); DSF20, disulfiram 20 mg/kg alone; PQ, paraquat 1.5 mg/kg; PQ+DSF5, PQ + disulfiram 5 mg/kg;

3 PQ+DSF10, PQ + disulfiram 10 mg/kg; PQ+DSF20, PQ + disulfiram 20 mg/kg. Statistical analysis: one-way

4 ANOVA with Tukey's multiple comparisons test. *P < 0.05, **P < 0.01, ***P < 0.001

5

6 Table 1: Effects of disulfiram co-treatment on oxidative stress markers in paraquat-induced nephrotoxicity.

Stress oxidative marker		**Cont**	**Oil**	**DSF20**	**PQ**	**PQ+ DSF5**	**PQ+ DSF10**	**PQ+ DSF20**	**P value PQ and Treat**
MDA	Mea± SEM	4.56±0.15	4.65± 0.21	5.96± 0.45	6.66± 0.45	4.98± 0.3	4.44± 0.31	6.09± 0.4	**PQ vs. PQ+DSF5** P=0.0284*
	Median	4.551	4.654	5.962	6.816	4.776	4.604	6.201	
	IQR	(4.23, 4.88)	(4.174, 5.145)	(5.071, 6.853)	(5.769, 7.496)	(4.371, 5.701)	(3.769, 5.034)	(5.247, 6.877)	**PQ vs. PQ+DSF10** P=0.0018** **PQ vs. PQ+DSF20** P=0.8976 ns
GPx	Mea± SEM	21.17±2.8	42.48± 4.19	38.8± 5.06	48.71± 5.34	17.72± 2.77	36.18±2.53	59.59±2.55	**PQ vs. PQ+DSF5**

	Median	22.02	45.95	38.45	48.7	15.95	34.12	60.59	P<0.0001****
	IQR	(15.97, 25.95)	(32.46, 50.77)	(29.16, 48.63)	(38.09, 59.34)	(12.69, 23.64)	(31.75, 41.63)	(54.43, 64.25)	**PQ vs. PQ+DSF10** P= 0.2605 ns **PQ vs. PQ+DSF20** P= 0.4178 ns
CAT	Mea± SEM	87.13±6.52	137.1± 8.21	290.5± 20.55	209.4± 6.84	225.1± 17.68	158.2±10.99	396.3±28.51	**PQ vs. PQ+DSF5**
	Median	85.00	138.3	315.0	211.7	225.0	171.7	371.0	P=0.9922 ns **PQ vs. PQ+DSF10**
	IQR	(73.3, 102)	(120.8, 152.8)	(242.5, 326.3)	(193.7, 224)	(185.8, 264.5)	(131.7, 178)	(346.7, 458.7)	P= 0.3065 ns **PQ vs. PQ+DSF20** P<0.0001****

1

2 Values represent mean ± SEM for MDA level, GPx activity, and CAT activity in renal tissue homogenates (n=5
3 animals per group). Cont, control; Oil, (vehicle); DSF20, disulfiram 20 mg/kg alone; PQ, paraquat 1.5 mg/kg;
4 PQ+DSF5, PQ + disulfiram 5 mg/kg; PQ+DSF10, PQ + disulfiram 10 mg/kg; PQ+DSF20, PQ + disulfiram 20
5 mg/kg. Statistical analysis: one-way ANOVA with Tukey's multiple comparisons test. *P < 0.05, **P < 0.01, ***P <
6 0.001

7

1 Table 2: Statistical analysis of Renal function biomarker in renal Tissue among Treated groups

Renal Function Biomarker		**Cont**	**Oil**	**DSF20**	**PQ**	**PQ+ DSF5**	**PQ+ DSF10**	**PQ+ DSF20**	**P value PQ and Treat**
BUN	Mea± SEM	19.4± 0.24	19.6± 0.24	21.2± 0.58	34.4± 4.17	20.4± 1.28	19± 0.44	24.6± 0.6	**PQ vs. PQ+DSF5** P<0.0001**** **PQ vs. PQ+DSF10** P<0.0001**** **PQ vs. PQ+DSF20** P=0.0055 **
	Median	19	20	21	36	22	19	24	
	IQR	(19,20)	(19, 20)	(20,22.5)	(26,42)	(17.5, 22.5)	(18, 20)	(24, 25.5)	
CR	Mea±SEM	0.64± 0.02	0.6± 0	0.64± 0.02	0.62± 02	0.6± 0	0.62± 0.02	0.64± 0.02	**PQ vs. PQ+DSF5** P>0.9999 ns **PQ vs. PQ+DSF10** P>0.9999 ns **PQ vs. PQ+DSF20** P>0.9999 ns
	Median	0.6	0.6	0.6	0.6	0.6	0.6	0.6	
	IQR	(0.6, 0.7)	(0.6, 0.6)	(0.6, 0.7)	(0.6, 0.65)	(0.6, 0.6)	(0.6, 0.65)	(0.6, 0.7)	
UA	Mea± SEM	87.13± 6.52	137.1 ±8.21	290.5± 20.55	209.4± 6.84	225.1± 17.68	396.3± 28.51	158.2± 10.99	**PQ vs. PQ+DSF5** P<0.0001****
	Median	0.9	0.9	0.6	1.8	0.7	0.6	1.6	

	IQR	(0.8, 1.2)	(0.85, 1.62)	(0.6, 1.15)	(1.3, 1.85)	(0.55, 0.75)	(0.5, 0.75)	(1.5, 1.8)	**PQ vs. PQ+DSF10** P<0.0001**** **PQ vs. PQ+DSF20** P>0.9999 ns

Values represent mean ± SEM for BUN, Creatin, and UA level (n=5 animals per group). Cont, control; Oil, (vehicle); DSF20, disulfiram 20 mg/kg alone; PQ, paraquat 1.5 mg/kg; PQ+DSF5, PQ + disulfiram 5 mg/kg; PQ+DSF10, PQ + disulfiram 10 mg/kg; PQ+DSF20, PQ + disulfiram 20 mg/kg. Statistical analysis: one-way ANOVA with Tukey's multiple comparisons test. *P < 0.05, **P < 0.01, ***P < 0.001

Supplementary Files

This is a list of supplementary files associated with this preprint. Click to download.

- Supplementaryfile.docx
- 1SupplementaryHEHistopathologycalfigures.pptx
- 2SupplementarytrichromHistopathologycalfigures.pptx
- 3SupplementaryPASHistopathologycalfigures.pptx